ABSTRACT

Title of thesis: THE EFFECTS OF LIQUID ALKANE FUEL STRUCTURE ON CATALYST-ENHANCED COMBUSTION

Grant Daniel Dubé
Master of Science, 2018

Thesis directed by: Professor Elaine Oran
Department of Mechanical Engineering

The U.S. Army is developing micro-combustors for use in soldier-portable power generation systems. Many of the challenges associated with micro-combustion can be potentially overcome using a catalyst, but the effects of the catalyst on ignition under the low temperature, atmospheric conditions seen in the field are not well understood. To better understand catalytic ignition phenomena under these conditions, a Catalytic Ignition and Emissions Tester (CIET) was developed and used to investigate the effects of liquid alkane fuel structure during catalyst enhanced ignition. Various mixtures of *n*-octane and *iso*-octane, as well as single component *n*-dodecane and *n*-hexadecane, were chosen as simple, surrogate test fuels to represent gasoline, jet fuel, and diesel, respectively. Fuel reactivity was shown to decrease with increased branching for all metrics tested while the effects of chain length were less definitive. The global apparent activation energies of all fuels tested were found to be in the range of 41-61 kJ/mol with 95% confidence, significantly lower than those previously reported for non-catalytic hydrocarbon combustion (>100 kJ/mol).

THE EFFECTS OF LIQUID ALKANE FUEL STRUCTURE ON CATALYST-ENHANCED COMBUSTION

by

Grant Daniel Dubé

Thesis submitted to the Faculty of the Graduate School of the
University of Maryland, College Park in partial fulfillment
of the requirements for the degree of
Master of Science
2018

Advisory Committee:
Professor Elaine Oran, Chair/Advisor
Professor Michael Gollner
Professor Peter Sunderland

Acknowledgments

I thank Dr. Elaine Oran, my adviser at the University of Maryland, for letting me join her group and for always providing guidance and encouragement when I needed it most.

I thank Dr. Ivan Lee, my adviser at the U.S. Army Research Lab (ARL), for mentoring me and for teaching me far more chemistry and catalysis than I ever thought I would know. I also thank him for valuing my opinions and making me part of the team.

This work was supported by the U.S. ARL. All experimental work was completed at the U.S. ARL in Adelphi, MD.

Thank you to Dr. Ryan Houim for teaching me the fundamentals of combustion and coding, both of which were integral to my research.

Thank you to all of the people at the U.S. ARL who provided me help over the past two years, particularly Dr. Zachary Dunbar, Dr. Luther Mahoney, and Mr. Ron Duane, for always being willing to lend a hand.

I thank Joe Chung for never hesitating to provide honest feedback on my work and presentations.

Thank you to Drs. Michael Gollner and Peter Sunderland for sitting on my advisory committee. Your flexibility with scheduling is greatly appreciated.

I thank Kerri Poppler James for helping me with all of the administrative work, from graduation paperwork to course scheduling.

Lastly, I thank those who are closest to me. To Shelley O'Conor, thank you

for always providing a listening ear and a welcome escape from my schoolwork. And to my family, thank you for always standing behind me and supporting me in my endeavors.

Table of Contents

List of Tables

List of Figures

Nomenclature

A	Arrhenius preexponential factor
ARL	Army Research Laboratory
Back-face	Face of the catalytic foam furthest downstream
CI	Confidence interval
DARPA	Defense Advanced Research Projects Agency
DOD	Department of Defense
E_a	Apparent activation energy
IPA	Isopropyl alcohol
JP	Jet propellant (JP-8, JP-5)
k	Apparent reaction rate (first order)
MS	Mass spectrometer
phi (ϕ)	Equivalence ratio
ppi	Pores per linear inch
P	Pressure
PRF	Primary reference fuel
R_u	Universal gas constant (8.31415 J/mol/K)
Run	A singular ignition event (25 runs were completed for each fuel)
S_A	Surface area
S_L	Laminar flame speed
SFC	Single Fuel Concept
sLpm	Standard liters per minute
syngas	Exhaust gas consisting of (H_2+CO)
t	Time
t_{idt}	Ignition delay time (time from fuel input to 10% O_2 conversion)
T	Temperature
T_{BF}	Back-face temperature
T_{ign}	Back-face temperature at fuel input

T_{SB}	Temperature at the front face of the rear heat shield
TE	Thermoelectric (device)
TPV	Thermophotovoltaic (device)
V	Volume
$\dot{V}_{air}$	Volumetric flow rate of air
X_{O_2}	molar concentration of oxygen

Chapter 1: Introduction

A Catalytic Ignition and Emissions Tester (CIET) has been developed to investigate the effect of fuel structure on the catalytic ignition of liquid alkanes at low temperatures (100-255°C) and atmospheric pressure, operating conditions which have not been well studied in the past. The key metrics measured by the CIET are temperature and oxygen conversion, both of which are metrics for fuel reactivity and can be used to calculate global apparent ignition kinetic parameters such as activation energy (E_a), reaction rate (k), and the Arrhenius pre-exponential (A). These experimentally determined parameters are extremely useful in the development of chemical models and micro-combustors for small scale, personal power generation.

1.1 The Single Fuel Concept (SFC)

The SFC, which mandates the use of a single fuel for operations in overseas theaters by all land and air forces, was implemented by the Department of Defense (DOD) in the late 1980's as a result of the problems experienced by the M1 Abrams battle tanks sent to Germany in 1981. The tanks were required to operate in a previously untested, low-temperature regime. At low temperatures ($\sim$-8°C), the heavy paraffin hydrocarbons (C_{15}+) in the tank's diesel fuel would congeal into a

waxy substance (waxing) and clog the fuel lines and filters. To prevent waxing from occurring, the diesel fuel was blended with other readily available fuels, notably Jet Propellant, in the form of JP-5 or JP-8, which contain an overall lighter distribution of paraffin hydrocarbons. To prevent the possible pitfalls associated with transporting and blending multiple fuels, the SFC was put into effect [1].

JP-8 is the single fuel of choice for the U.S. Army and is the second most transported item in the field next to water [2]. As such, there are a number of benefits, logistical and otherwise, to using JP-8 as the single fuel. These benefits include: ease of production, distribution and handling; improved long term storage and cold weather performance; and reduced wear on the vehicle's powertrain. JP-8 is JET A-1, a kerosene grade, commercial jet fuel produced to strict international standards, with the addition of three mandatory additives to inhibit icing in the fuel system (di-ethylene glycol monomethylether), improve corrosion resistance and lubrication (typically contains dilinoleic acid which adheres to metal and forms a thin surface film), and improve static discharge (Stadis®450) [3].

Despite the additives mentioned above, there are still two major problems encountered when using JP-8 in the field. The first is insufficient lubrication in ground vehicles operating at elevated temperatures. The higher ambient temperatures found in Afghanistan decreased the viscosity of the fuel, thus decreasing its ability to lubricate key powertrain components, namely the fuel pump. Poor lubrication coupled with the added weight of extra armor for protection against improvised explosive devices resulted in engine failures after only 1,000-2,000 miles [4].

The second major problem encountered when using JP-8 is poor transient and

long-term operation of small fuel conversion devices. JP-8 has an energy density (lower heating value) of 11 kWh/kg [5]. The energy density of the soldier's main electrial energy source, a Li-ion battery, is only 0.15 kWh/kg [6]. Consider this scenario in which a soldier needs 35 W continuously for four days (96 h). This results in 8.4 L and 22.4 kg of Li-ion batteries. If using a portable, JP-8 powered combustor, such as the Defense Advanced Research Projects Agency (DARPA) Palm Power, the resulting volume is 4.2 L with a mass (wet) of only 2.9 kg [7]. Using portable combustors to provide power at the soldier and squad (8-12 soldiers) levels would greatly improve the soldier's capabilities as well as increase the overall utility of JP-8 on the battlefield.

1.2 Micro-combustor Challenges

Micro-combustors, as opposed to meso-scale and large-scale combustors, present a unique set of challenges and problems. As the dimensions of the combustor become smaller, the ratio of surface area to volume ($S_A : V$) becomes larger, which leads to increased heat loss through the walls of the combustor. The increased heat loss results in less a less stable flame or even the extinction of a flame due to thermal or radical quenching. Thermal quenching dominates at low temperatures ($\sim$500 K) and will extinguish a flame when the heat of combustion is less than the heat loss through the walls. Radical quenching dominates at high temperatures ($\sim$1000 K) [8] and this results from the formation of stable products through termination reactions that occur when radicals collide with walls. In combustors with smaller

$S_A : V$ ratios, radical quenching prevents a buildup of free radicals which could lead to an explosion. Conversely, if all the radicals are terminated at the wall, then the combustion stops and the flame is extinguished [9].

Short residence times (also called contact times) are another problem commonly encountered in micro-combustors. As the dimensions of the combustor decrease, increased flow rates are required to maintain a given power output. High flow rates lead to a third type of quenching, blowout. Blowout occurs at high flow rates when the flame speed is less than that of the incoming reactants, and the flame is physically blown out of the combustor. When there is not enough time for the fuel-air mixture to react, short contact times can also lead to incomplete combustion. This issue is exacerbated by the fact that heavy hydrocarbons, like those found in JP-8 and diesel, do not vaporize easily and require preheating as well as more time to ignite. Preheating increases the energy input requirement of a combustor with an already small power output. In fact, Lee *et al.* [10] has shown that the CUBE Micro-Furnace coupled with a thermo-electric (TE), a device that produces electricity as a result of a temperature gradient through the Seebeck effect [11], requires upwards of 8 hours to have a positive power output due to its relatively high input requirements when using JP-8.

1.3 Catalysts

Many of the problems discussed in the previous section can be addressed by using a catalyst to aid the combustion process. In small systems, catalysts are typi-

cally applied directly to the walls of the combustor or impregnated on ceramic foams and placed inside the reactor. This is done in order to crack, or break up, the large incoming fuel molecules so that they react faster. Catalysts provide an alternative reaction mechanism that requires less energy to activate, thus lowering E_a needed to initiate combustion while increasing k. Decreasing E_a facilitates low-temperature ignition and lower fuel-air preheat, thus reducing the input power requirement during startup, while increasing k decreases the residence time required for complete combustion to occur. In addition, combustion occurs on the surface of the catalyst, which anchors the flame: preventing blowout and providing a fixed heat source conducive to integration with TE and thermophotovoltaic (TPV) devices [9].

While using catalysts can help solve some of the more fundamental problems found in micro-combustors, they also provide their own set of problems, namely, deactivation of the catalyst and oil formed by pyrolysis. Deactivation is a problem that occurs when active reaction sites on the catalyst become poisoned or blocked. Coke, excess carbon (soot) resulting from incomplete combustion, and sulfur are common causes of deactivation on "traditional" catalysts, such as nickel and platinum. The relatively high sulfur content of JP-8 (400-3,000 parts per million by weight (ppmw)) [12] as compared to gasoline (10-95 ppmw) and diesel (15-500 ppmw) [13], provides a particular challenge when developing catalysts.

Pyrolysis oil formation, the second problem mentioned above, occurs when the combustor's operating temperature or pressure is too high and insufficient oxygen is supplied to undergo complete oxidation. The absence of oxygen results in an oil vapor (pyrolysis oil) that can condense into a thick, liquid oil, potentially restricting

or even stopping the flow of exhaust gases downstream of the combustor and causing a catastrophic failure.

1.4 Surrogates

JP-8 and other transportation fuels are complex mixtures of hydrocarbons that can be difficult to work with when trying to understand fundamental combustion characteristics and trends through experiments and modeling. A common way of combating this complexity is by using a surrogate fuel to represent the real fuel. Generally, surrogates should contain the minimum number of components that will emulate the real fuel's combustion characteristics [14]. A lot of work has been done to develop surrogates for transportation fuels [15–20]. There is, however, still a gap in the literature when it comes to understanding the combustion phenomena of possible surrogate transportation fuels for low-temperature, atmospheric, catalytic combustion.

The objective of this thesis is to expand the working knowledge of low temperature, atomospheric, catalytic combustion by investigating six possible surrogate fuels for three prevalent transportation fuels: JP-8, gasoline, and diesel. This was done by looking at the effect of the hydrocarbon chain length and branching on ignition characteristics. While there are many factors to consider when picking a surrogate, matching the C/H ratio of the surrogates to the real fuel is important [22, 23]. The hydrocarbon distribution ranges shown in Fig. 1.1 were used to match the average C/H ratio for the three fuels of interest. As a result, n-$C_{12}H_{26}$, n/iso-C_8H_{18},

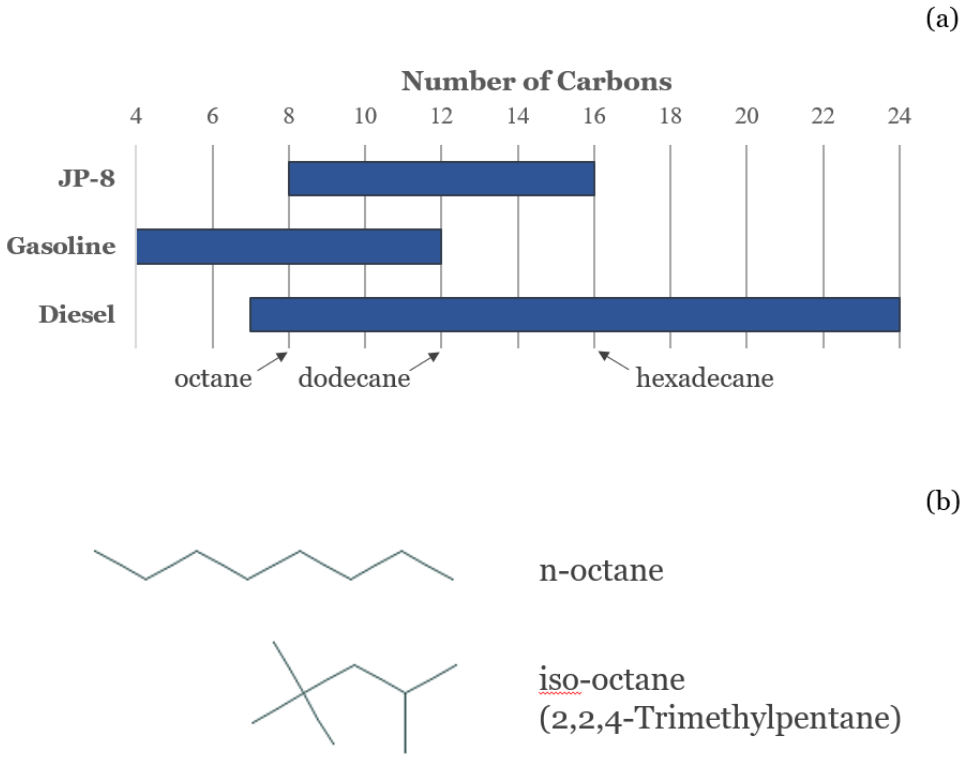

Figure 1.1: (a) Typical hydrocarbon distribution ranges for JP-8 [3], gasoline, and diesel [21]. (b) molecular structure of n-octane and iso-octane.

and n-$C_{16}H_{34}$ were chosen as surrogate fuels to represent JP-8, gasoline, and diesel, respectively.

Chapter 2: Literature Review

This review summarizes relevant information on the ignition of alkanes (also called paraffins), specifically the effects of fuel branching and length on ignition characteristics for both non-catalytic and catalytic combustion systems. The characteristics of interest that are commonly measured are minimum ignition temperature ($T_{ign,min}$), ignition delay time (t_{idt}), and laminar flame speed (S_L), all of which are indicative of fuel reactivity. When using these quantities to compare fuels, smaller values for $T_{ign,min}$ and t_{idt} and larger values for S_L indicate a more reactive fuel.

2.1 Non-Catalytic Combustion

Shen *et al.* [24] conducted shock-tube experiments for *n*-alkanes (C_7-C_{14}) in air at multiple equivalence ratios and at temperatures and pressures ranging from 786-1396 K to 9-58 atm, respectively. Within experimental error, little difference was observed in ignition delay times for the different fuels for ignition temperatures less than 1000 K (1000/T = 1.0), which were in good agreement with the models from Curran *et al.* [25], Westbrook *et al.* [26], Ranzi *et al.* [27], and Biet *et al.* [28]. The results from the experiment and models are compared in Fig. 2.1 [24]. This agreement was attributed to the fact that even though the fuel content in the fuel-air

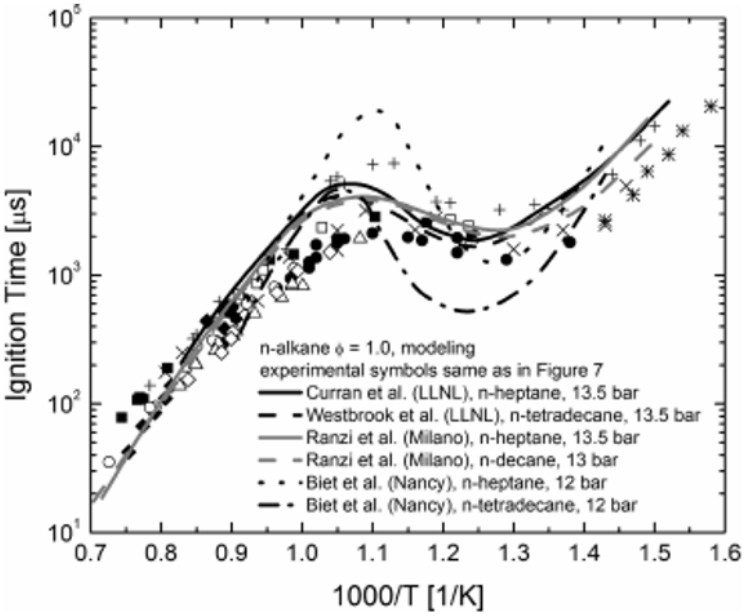

Figure 2.1: Comparison of ignition delay times of shock-tube data and kinetic models for various lengths of n-alkanes [24].

mixture changes due to differences in chain length, the overall carbon content of the mixture stays about the same. For example, the carbon contents for n-heptane and n-tetradecane in stoichiometric air differ by only 3%.

Tekawade and Oehlschlaeger [29] looked at the effects of fuel structure on ignition characteristics for a a range of higher alkanes (C_6-C_{16}) via spray ignition in a constant volume spray combustion chamber. The operating ranges of temperature and pressure studied were 650-825 K and 1-4 MPa, respectively. Contrary to the work above, these experiments showed that ignition delay decreased (more reactive) with increasing chain length. This observation is corroborated by the work of Mendelson [30], who compared ignition data recorded by the Ignition Quality Tester at the U.S. Naval Academy in Annapolis, MD from multiple fuels, notably

n-heptane, *n*-decane, and *n*-hexadecane. Furthermore, Tekawade and Oehlschlaeger found that lightly branched alkanes behaved similarly to their normal counterparts, while highly branched alkanes exhibited longer ignition delay times (less reactive). Based on these results, the authors concluded that *n*-alkanes can be used as surrogates for lightly branched alkanes. In addition, highly branched alkanes, *iso*-octane and *iso*-cetane were found to have a very distinct two-stage ignition at all pressures tested. Two stage ignition was also observed for *n*-alkanes at P=1 MPa, but single-stage ignition was observed at higher pressures of P=2.14, 4.0 MPa for the same compounds. Boiling points of the different fuels were not found to have an influence on reactivity.

Bugler *et al.* [31] investigated the influence of fuel structure on ignition delay times using a shock-tube and a rapid compression machine at pressures of 1, 10, and 20 atm, and at equivalence ratios of 0.3, 0.5, 1.0, and 2.0 in simulated air. It was found that *n*-pentane was more reactive than *iso*-pentane across all operating conditions up to 950 K. Simulated ignition delay times using an extended chemical model were in good agreement with those that were experimentally obtained.

Li *et al.* [32] also used a combination of modeling and experiments to determine the effect of fuel structure on flame speed using *n*-butane and *iso*-butane at pressures of 1, 2, 5, and 10 atm at multiple equivalence ratios ranging from 0.7-1.7. The experimental setup involved using a 2.77 L constant-volume reactor with a 9 L premixing vessel and an ignition coil to initiate combustion. A Schillerian imaging system was used to measure the speed of the spherical flame as it progressed through the fuel-air mixture. Both the model and experiment reported slower flame speeds

for the branched fuel. Moreso, mixtures of *n*-butane *iso*-butane were tested for *n*:*iso* ratios of 0.3:0.7, 0.5:0.5, and 0.7:0.3, and it was found that flames speeds gradually decreased with increasing *iso*-butane ratio. A gradual increase of ignition delay times with increasing *iso*-butane ratio was also reported, again indicating that branching decreases reactivity. These observations are consistent with those of Davis and Law [33]. This fact is attributed to the easy production of H atom from *n*-butane decomposition and the dominance of the reactive C_2 chemistry.

2.2 Catalytic Combustion

There are far fewer studies covering the effects of alkane fuel structure on ignition characteristics during complete, catalytic combustion. Much of the information available on the catalytic combustion of alkanes is for partial oxidation conditions (incomplete combustion) with the purpose of producing syngas (H_2+CO) [34–42]. *Iso*-octane was found to be more reactive (lower ignition temperatures) than *n*-octane under partial oxidation conditions with a rhodium (Rh) catalyst [34, 42]. This is the opposite of what is commonly seen in non-catalytic, complete combustion.

For small *n*-alkanes (C_1-C_4), Veser *et al.* studied the effect of chain length on ignition temperature using a flow tube reactor (varied fuel flow rate, air flow rate=3 sLpm) coupled with a platinum (Pt) foil catalyst over a temperature range of 150-600°C depending on the fuel. Fig. 2.2 [43] shows (1) decreasing ignition temperature with increasing equivalence ratio and (2) decreasing ignition tempera-

ture with increasing chain length. The first observation was attributed to the likely event of site blocking by O_2. The second can be traced back to the correlation of the activation of the hydrocarbon with the C-H bond strength (also seen in [44]). It is mentioned that surface ignition and C-H bond strength are not linearly dependent. To get a more complete understanding of the process governing differences in catalytic ignition, other factors such as sticking coefficients and site competition must be considered. By comparing catalysts, Veser *et al.* [43] reported highly reproducible ignition temperatures for Pt and Palladium (Pd) but not for Rh and Iridium (Ir). For Ir, results had more scatter in the data and depended strongly on the conditions of previous experiments. For these catalysts, surface ignition temperatures increase with an increasing metal-O_2 bond energy in order of: Pt<Pd<Rh<Ir. Varying the air flow rate from 1-6 sLpm had no effect on the observed minimum ignition temperatures.

Bijjula and Vlachos [45] studied the effect of fuel structure on ignition temperature for JP-8 and potential surrogates (alkanes tested: *iso*-C_8, *n*-C_{12}, and *n*-C_{14}) in a packed-bed flow reactor (air = 0.2 sLpm) over a temperature range of ∼150-240°C with a Pt catalyst. When comparing the two *n*-alkanes tested, they found that ignition temperature increased with increasing carbon chain length. The differences seen between this study and the one conducted for smaller *n*-alkanes by Veser *et al.* were attributed to a difference in sticking coefficients between the fuels. The sticking coeffeicient is defined as the ratio of molecules that stick to the surface of the catalyst to the number of impinging molecules [46]. As it was with non-catalytic combustion, there seems to be no relationship between boiling point and ignition

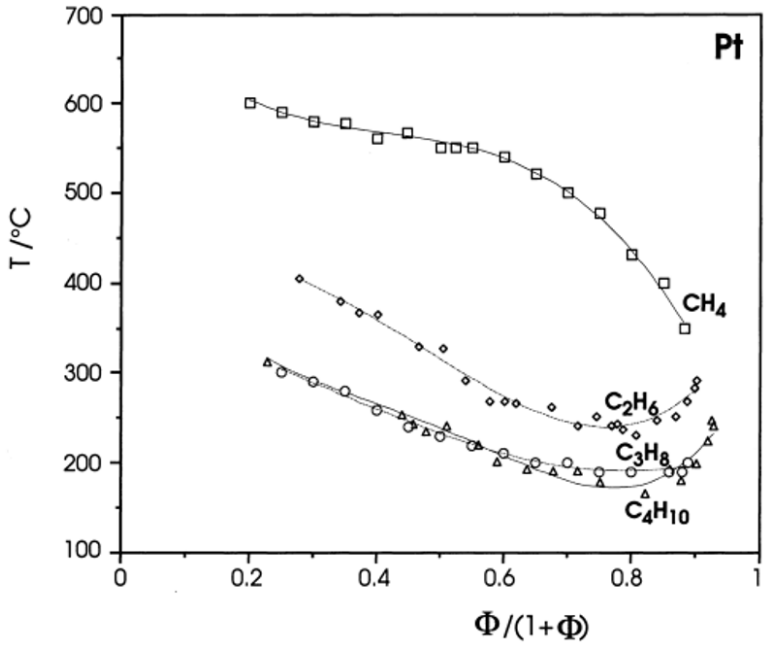

Figure 2.2: Comparison of minimum igntition temperatures for small *n*-alkanes as a function of (modified) equivalence ratio [43].

temperature.

2.3 Apparent Global Activation Energy

Although ignition temperatures and delay times are commonly measured, activation energy is often not calculated or reported [47]. The apparent global activation energy is the amount of energy required to ignite a fuel under the given experimental conditions. When reported, there seems to be significant variation from experiment to experiment. Wierzbicki *et al.* studied the combustion behavior of propane over Pt and Rh catalysts in a meso-scale, swiss-roll style combustor. Values of E_a of 13.8 kJ/mol and 74.7 kJ/mol were reported for propane over Pt and Rh, respectively [48],

while Veser *et al.* reported an apparent activation energy of about 80 kJ/mol with the same fuel and catalyst under comparable conditions using Pt foil as a catalyst [43]. Williams and Schmidt reported an average value of E_a=78 kJ/mol for C_4, C_8, and C_{10} alkanes under partial oxidation conditions using a Rh catalyst [42]. For non-catalytic hydrocarbon combustion, Westbrook and Dryer [49] found that an appropriate E_a was 126 kJ/mol based on the lower value reported by Fenn and Calcote (109 kJ/mol) [50] and the higher value reported by Walker and Wright (167 kJ/mol) [47].

The variations in apparent activation energies reported above may be partially accounted for by considering compensation effects. Bond (1999) explained that compensation in heterogeneous (surface reactions) catalysis takes the form of a linear correlation between activation energy and pre-exponential factor $ln(A)$, and that the apparent Arrhenius parameters for many different Pt and palladium (Pd) catalysts lie close to a common compensation line. Since alkane activation requires endothermic dehydrogenative chemisorption, apparent global activation energies will often times exceed true activation energies. This compensation effect accounts for the dependence of global apparent activation energy on alkane chain length as well as the high values sometimes reported [51].

Chapter 3: Experimental Methods

This chapter provides details on the Catalytic Ignition and Emissions Tester (CIET) as well as the procedure and methods used to study the ignition characteristics of liquid hydrocarbons during low temperature, atmospheric, catalytic combustion.

3.1 Catalytic Ignition and Emissions Tester

The CIET, diagrammed in Fig. 3.1, consists of three major parts: fuel-air input, a reactor, and exhaust processing. The fuel-air input system consists of a MKS 946 system controller connected to two MKS MASS-FLO® controllers allowing for independent control over nitrogen (10,000 sccm) and oxygen (5,000 sccm) flow rates. An inline pressure guage was placed on the incoming gas stream. No back-pressure was observed during experimentation, confirming a reactor pressure of 1 atm. Liquid fuel is stored in a 40 mL glass vial and the flow rate is controlled with a positive displacement pump and controller (Valco Insturments model: M6 CP-DSM). Preheating of the unmixed fuel and air is achieved by variac controlled heating tape with a type-K thermocouple for monitoring. All temperature measurements were made and recorded using type-K thermocouples connected to a Pico

TC-08 USB thermocouple data logger.

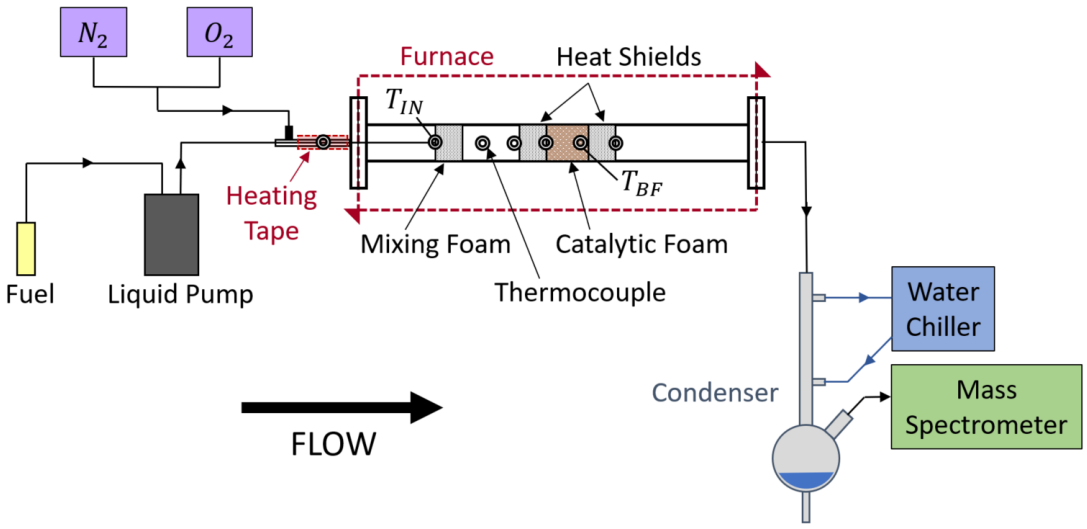

Figure 3.1: Diagram of the CIET.

The reactor is a 28 mm (ID) x 33 cm long Inconel® tube with Swagelok® fitted vacuum flanges (sealed by copper gaskets) on either end. It is important to note that N_2 and O_2 enter the reactor at the vacuum flange through a $\frac{1}{4}$ in tube, while the $\frac{1}{16}$ in fuel tube, concentric with $\frac{1}{4}$ in tube, passes through the vacuum flange, into the reactor, and into an 80 pores per linear inch (ppi) ceramic-alumina foam (ceramic foam or foam), labeled "Mixing Foam" in Fig. 3.1. When the preheated fuel reaches the mixing foam, it spreads out due to the foam's high porosity, mixes, and becomes entrained with the incoming gases. A thermocouple is placed to record the temperature at the end of the fuel tube (T_{IN}) by wrapping it around the fuel tube and inserting it through the vacuum flange. When the liquid fuel makes contact with the thermocouple, a sudden drop in temperature occurs. The time at which

this happens is defined as t=0 s. There are three more ceramic foams located inside the reactor: two 20 ppi foams (25 mm D x 12.5 mm L) and another 80 ppi foam (25 mm D x 25 mm L) that contains the catalyst. The 20 ppi foams are placed on either side of the catalytic foam to prevent excessive heat loss during ignition. All foams were wrapped in fiber paper to provide a tight seal against the reactor wall. There are five thermocouple ports centered along the length of the reactor and spaced 20 mm apart. The key thermocouples are located at the mixing foam and at the back-face of the catalyst, where ignition was observed and are designated as T_{IN} and T_{BF}, respectively, in Fig. 3.1. Please note that the back-face thermocouple lies just to the left of the back-face of the catalyst, as depicted, due to a minor mismatch in spacing of the thermocouple ports and lengths of the ceramic foams. The reactor itself is located inside a three-zone, programmable, box furnace.

Once the exhaust gases leave the reactor, they are routed through a water-chilled condenser to a Hamilton Sundstrand MGA 1200EC mass spectrometer (MS) capable of detecting the following nine gases simultaneously: H_2, He, CO, CH_4, C_2H_4, N_2, C_2H_6, CO_2, and O_2. Gas concentrations (mole %) are calculated and logged with 1 s resolution by the MS using proprietary Prime software. This MS is specially fitted with a co-axial cable port that can be used to directly read the MS voltage (0-5 V signal) for O_2. A simple LabView® program was used in conjunction with a LabJack U3-HV USB DAQ to log the O_2 voltage with 100 ms resolution. None of the other gases detected by the MS have the same molecular weight as O_2, so the voltage signal corresponds directly to the amount of O_2 present in the exhaust stream (higher voltage indicates more O_2).

3.2 Procedure

The CIET was used to test the ignition characteristics of 6 different fuels. The first set of fuels consisted of four mixtures of octane in the following n:iso volumetric ratios: 100:0, 30:70, 70:30, and 0:100 to investigate the effect of fuel branching, while a second set, n-dodecane and n-hexadecane, were tested and compared to n-octane to investigate the effect of chain length. Ignition was observed a total of 25 times for each fuel, five runs each at five different temperatures.

Before taking any data, the CIET was first primed by lighting off the catalyst at operating conditions and allowing the the back-face temperature (T_{BF}) to reach 1100°C. By allowing the catalyst and reactor to heat up, the variability due to a "cold" first run was avoided. Priming also served as a check to ensure all equipment functioned as expected. After priming, a cool-down sequence was performed. N_2 and O_2 at 10 sLpm and 3 sLpm, respectively, were flowed through the reactor for 3-4 min to allow the excess heat to dissipate. The flow rates were then adjusted to simulate air (79% N_2, 21% O_2) at a total flow rate of 9 sLpm, and the reactor was allowed to reach steady state. When necessary, the furnace temperature was adjusted to achieve the desired T_{BF} prior to ignition.

With T_{BF} at the desired steady state ignition temperature, data collection was initiated(MS, thermocouples, and O_2 voltage) and fuel was input, signified by a drop in T_{IN} (see Appendix A for example T_{IN} plot). The O_2 voltage, plotted in real time, was observed to ensure ignition. A successful ignition was characterized by a continuous drop in O_2 voltage and continuous rise in T_{BF}. Temperatures greater

than 1200°C were avoided to prevent catalyst vaporization. A typical run would last 1-2 min, after which data acquisition was stopped and fuel was cut. The cool down sequence was performed to prepare the CIET for the next run. After five runs at a given temperature, T_{BF} was increased 5-10°C and the process was repeated. To help avoid the high temperatures mentioned previously, the CIET was operated with the furnace slightly open (1 in) to prevent excessive heat build up following ignition. All temperatures reported are from the radial center of the reactor. The air flow rate ($\dot{V}_{air}$) was set to 9 sLpm for all experiments and the fuel flow rate was varied to achieve an equivalence ratio (ϕ) of 0.5, where ϕ is defined as the actual carbon to oxygen ratio (C/O) ratio divided by the stoichiometric C/O ratio:

$$\phi = \frac{(C/O)_{act}}{(C/O)_{stoich}} \tag{3.1}$$

An ignition was considered failed if the O_2 voltage did not begin to continuously drop within in 20 s of fuel input. After a failed ignition was observed, fuel was cut and the furnace was used to increase T_{BF} 50°C. Fuel was input and the catalyst ignited to ensure any excess fuel left in the reactor was burned off before the next run.

Any time the fuel being tested was changed, the fuel line was disconnected from the reactor and the pump and lines were purged with 99% isopropyl alcohol (IPA). The new fuel was used to purge the IPA and the line was then reconnected to the reactor, ready for the next run.

3.2.1 Equipment Delay

The time for the exhaust gases to travel from the back-face of the catalyst to the MS and be detected was calculated in order to report accurate ignition delay times (t_{idt}). Simulated air was fed into the reactor at 9 sLpm at operating conditions (T_{BF}=120°C) [1]. With the O_2 voltage reading at steady state, data collection was started and allowed to run for 20 s, at which point the flow of oxygen was cut and a drop in voltage was observed. The time of the O_2 cut was recorded by hand. The flow of O_2 was then reinstated and conditions were allowed to return to steady state. This process was repeated a total of 16 times: 8 each for the full CIET setup (Δt_F) and short CIET setup (Δt_S), as depicted in Fig. 3.2.

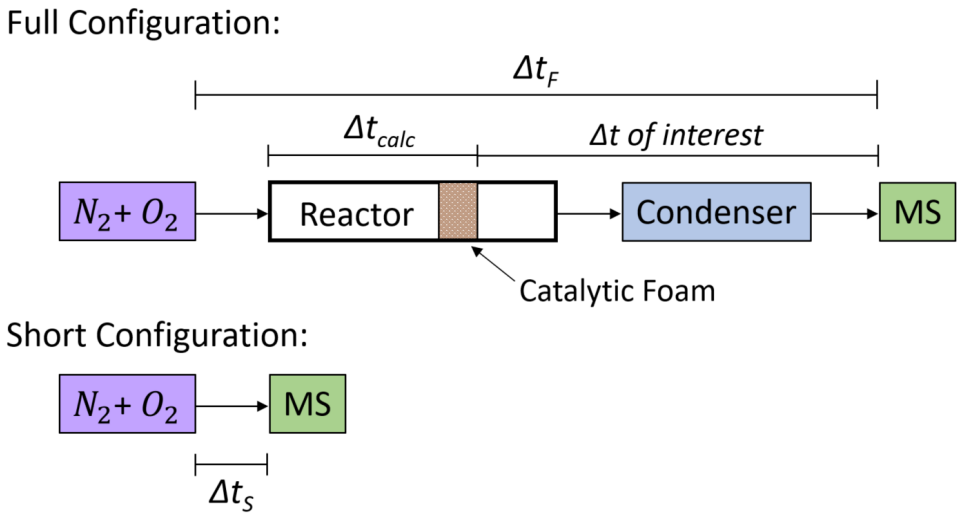

Figure 3.2: Diagram showing the various configurations used to measure the equipment delay time (Δt *of interest*).

[1] This temperature was initially chosen because it is representative of the operating temperatures for the octane mixtures. This test was later repeated for T_{BF}=230°C (representative of hexadecane) with no observable differences.

A MATLAB® script was used to process the recorded data and find the time at which the O_2 voltage dropped for both the full and short setups as well as to calculate the theoretical time for the air to flow from the reactor inlet to the back-face of the catalyst (Δt_{calc}). With this data, an equipment delay (Δt *of interest*) of 2.3±0.2 s was calculated with 95% confidence.

3.3 Catalyst Material

A Pt catalyst was selected for experimentation because it is well studied, versatile, and has been shown to have low run to run variability during ignition [43]. The structure of the catalyst consists of an 80 ppi, cylindrical, ceramic foam monolith (25 mm D x 25 mm L). The high surface area of the ceramic foam allows for a large number of catalyst active sites. An α-alumina (Al_2O_3) wash was applied to the ceramic foam (3.5 wt%) as a base material for the catalyst. A $Pt(NO_3)$ solution was then used to impregnate the platinum onto the alumina base for a final Pt loading of 2.5 wt.%. The details of catalyst preparation can be found in Appendix B.

Chapter 4: Experimental Results and Analysis

All results presented are for the following operating conditions: ϕ=0.5, $\dot{V}_{air}$=9 sLpm, and pressure (P)=1 atm. The fuel flow rate was varied to account for the various fuel compositions. Selected runs are shown for comparison. The ignition temperature and corresponding ignition delay time can be found in Appendix C. In the early stages of experimentation, a number of other operating conditions were tested. The conditions where deemed "failed" if they were not conducive to producing meaningful results. Appendix D lists a select number of operating conditions and their reasons for failure.

4.1 Chain Branching Effects

The O_2 voltage signal recorded from the mass spectrometer was normalized so that 0 indicates no O_2 conversion and 1 indicates full O_2 conversion for the conditions studied. The O_2 conversion was measured as a function of time for four different fuel-air mixtures in order to investigate the effects of chain branching on fuel reactivity during catalytic ignition. The fuels compared were mixtures of octane in the following ratios (n:iso): 100:0, 70:30, 30:70, and 0:100. Fig. 4.1 compares the O_2 conversion for the four octane mixtures tested and shows how higher ignition

temperatures correlate to faster conversion. The dependence of O_2 conversion on temperature reveals that the heterogeneous combustion reactions that initially take place are kinetically limited as opposed to diffusion limited. If diffusion limited, the mixture would ignite at the same rate regardless of temperature.

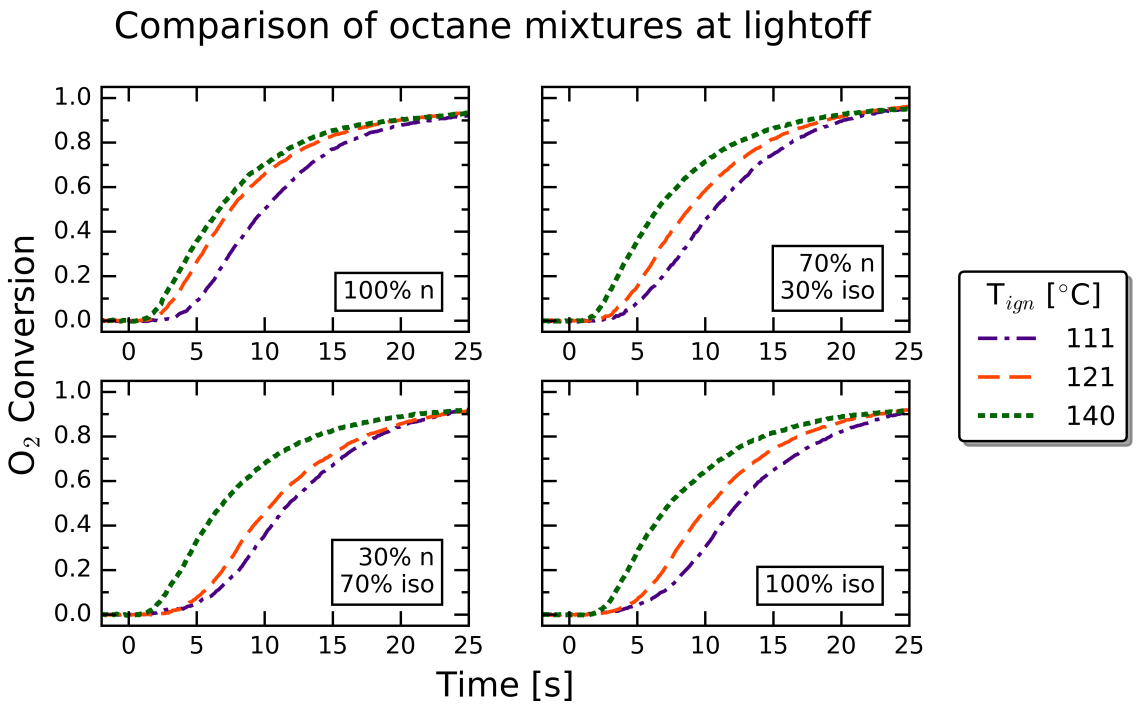

Figure 4.1: O_2 conversion comparison of octane mixtures at different lightoff temperatures for ϕ=0.5, $\dot{V}_{air}$=9 sLpm, P=1 atm.

To examine the relative reactivity of the fuels, Figs. 4.2 and 4.3 compare O_2 conversion for the four mixtures at the two different ignition temperatures. The lines in Fig. 4.3 compared to Fig. 4.2 are grouped much more tightly, suggesting that chain branching has more of an effect on O_2 conversion, and thus fuel reactivity, at lower ignition temperatures. At the lower ignition temperatures, increasing the content of *iso*-octane gradually lowers the reactivity of the fuel; one fuel does not

appear to dominate ignition, as indicated by the incrementally spaced conversion lines in Fig. 4.2. These observations are in good agreement with the literature previously discussed [32, 33].

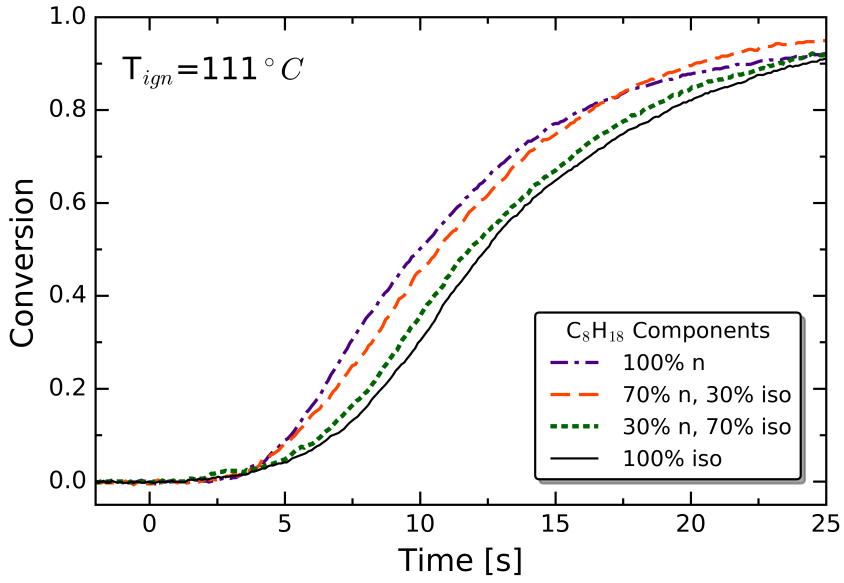

Figure 4.2: O_2 conversion comparison of octane mixtures at T_{ign} ≈110°C for ϕ=0.5, $\dot{V}_{air}$=9 sLpm, P=1 atm.

Intermediate species, notably H_2 and CO, were observed during ignition for all octane mixtures and can be seen in Figs. 4.4-4.7. The amount of H_2 and CO produced appear to change with the *n*:*iso* mixture ratio. The concentration of these species during their peak for pure *iso*-octane is about twice that of what is seen for pure *n*-octane. H_2 and CO concentrations for the 70*n*:30*iso* and 30*n*:70*iso* mixtures follow suit and lie somewhere in between the pure component fuels, with the relative concentrations of these minor species being arguably higher for the 70*n*:30*iso* mixture. The creation of H_2 and CO during lean hydrocarbon oxidation

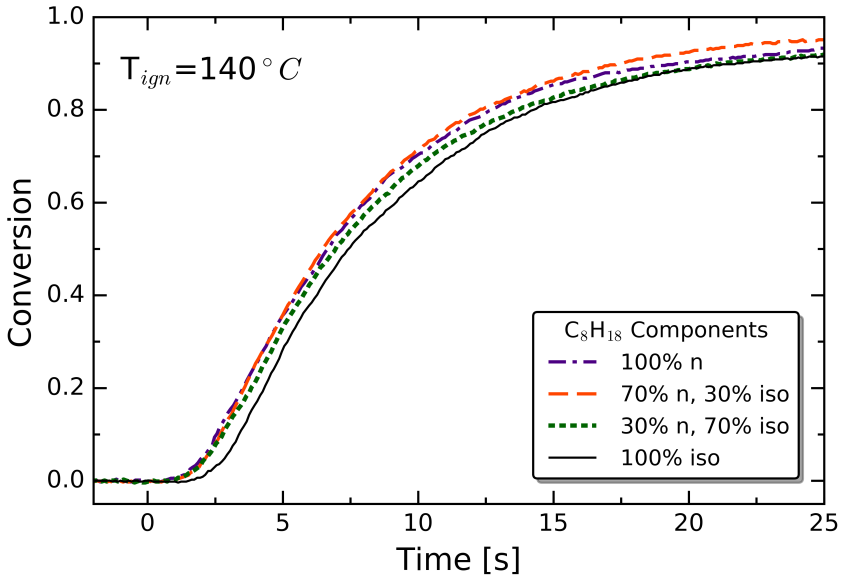

Figure 4.3: O_2 conversion comparison of octane mixtures at T_{ign} ≈140°C for ϕ=0.5, $\dot{V}_{air}$=9 sLpm, P=1 atm.

overt Pt was also seen by Badra and Masri. The authors noticed radicals such as O, OH, CH_3, HCO form very close to or on the catalyst's surface but decay very quickly to yield peaks in H_2 and CO [52].

The equilibrium distribution of major combustion products, after oxidation of H_2 and CO (signified by a drop in concentration), for *iso*-octane seen in 4.7 was compared to a modeled equilibrium distribution computed using Cantera, an open-source chemical kinetics software. Pure *iso*-octane and air at ϕ=0.5 were equilibrated using a 171-species skeletal mechanism for primary reference fuel (PRF) [53]. The computed mole fractions of the combustion products were then corrected to account for the absence of water in the experimental data. Fig. 4.8 shows good agreement between the model and experiment and confirms that complete

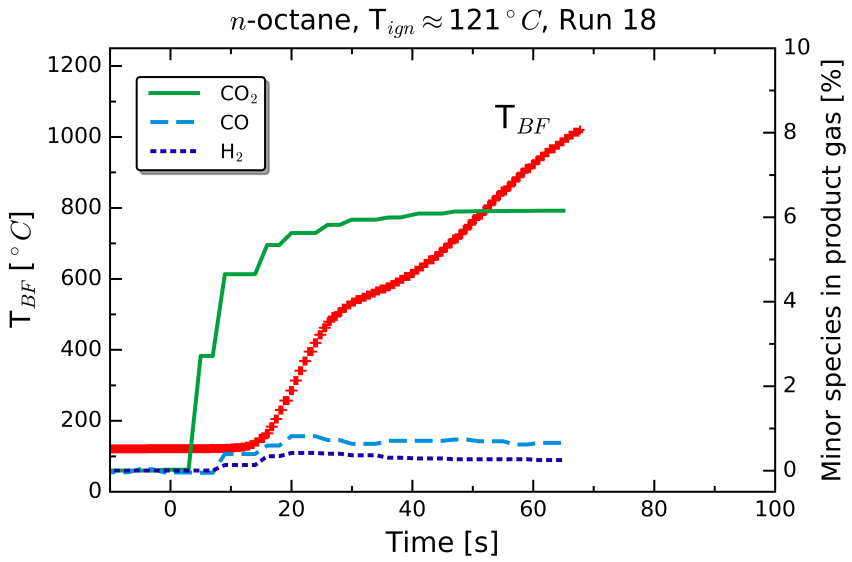

Figure 4.4: Minor species and T_{BF} of pure n-octane, Run 18: ϕ=0.5, $\dot{V}_{air}$=9 sLpm, P=1 atm.

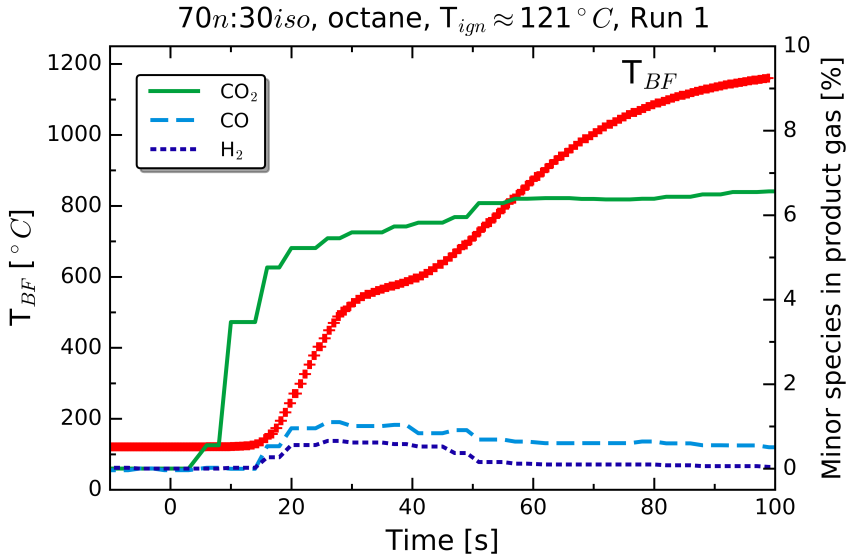

Figure 4.5: Minor species and T_{BF} of octane mixture (70n:30iso), Run 1: ϕ=0.5, $\dot{V}_{air}$=9 sLpm, P=1 atm.

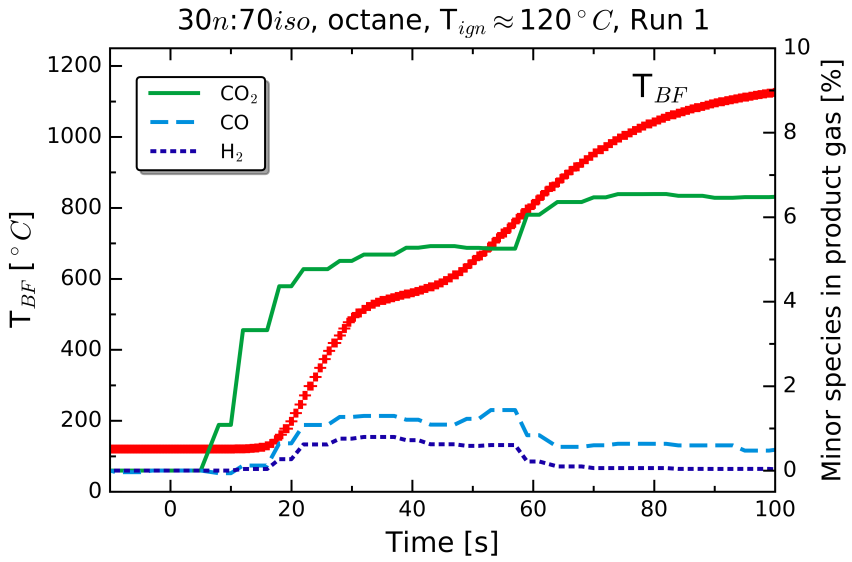

Figure 4.6: Minor species and T$_{BF}$ of octane mixture (30n:70iso), Run 1: ϕ=0.5, $\dot{V}_{air}$=9 sLpm, P=1 atm.

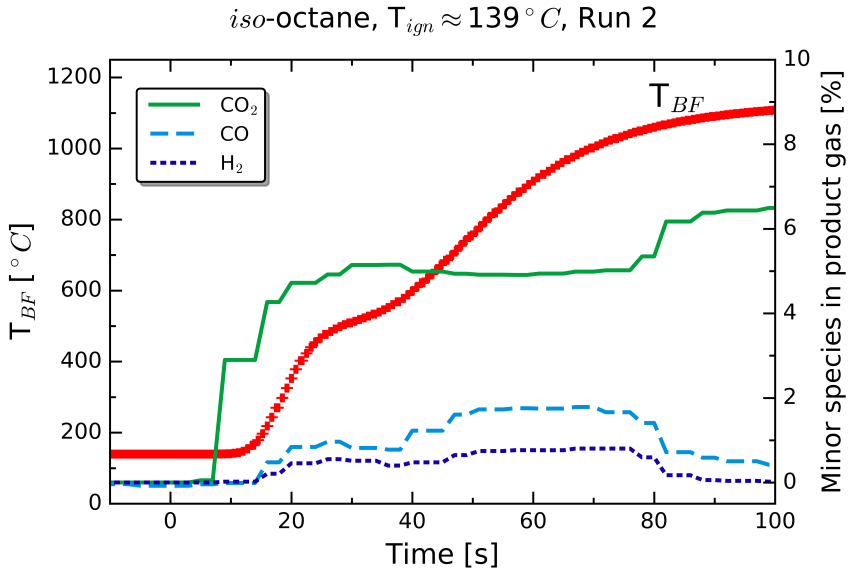

Figure 4.7: Minor species and T$_{BF}$ of pure iso-octane, Run 2: ϕ=0.5, $\dot{V}_{air}$=9 sLpm, P=1 atm.

combustion does eventually occur despite the short residence time between the fuel-air mixture and catalyst (∼60 ms).

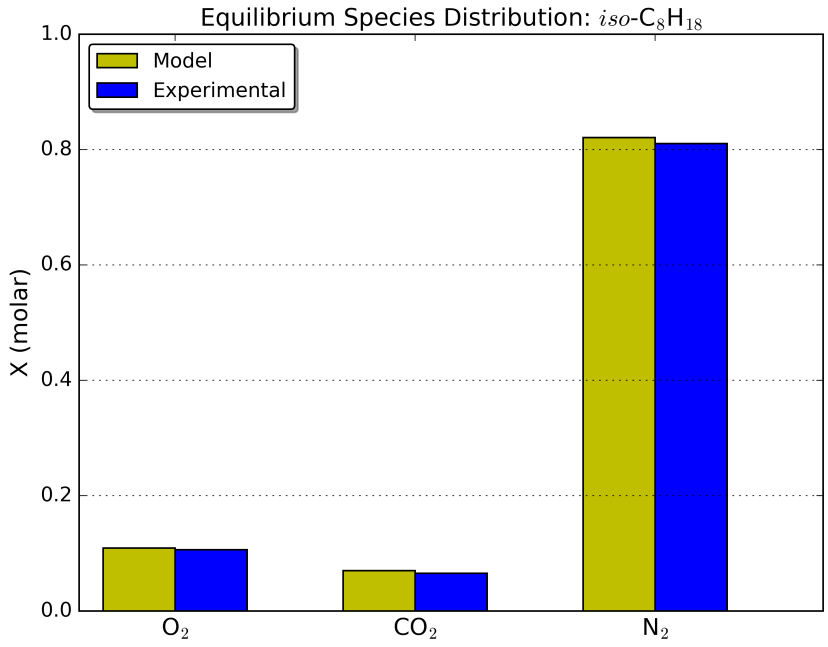

Figure 4.8: Model comparison of combustion product distribution for pure *iso*-octane. Experimental conditions for Run 2: T_{ign}=139°C, ϕ=0.5, $\dot{V}_{air}$=9 sLpm, P=1atm. Initial conditions for calculation: ϕ=0.5, T=27°C, P=1 atm.

The minimum ignition temperature ($T_{ign,min}$) for each fuel was defined as the lowest back-face temperature for which ignition occurred within 20 seconds of fuel input. Successful ignition was characterized by a small drop and then steady rise in back-face temperature, whereas the back-face temperature during an unsuccessful ignition would drop and stay approximately constant. Fig. 4.9 shows $T_{ign,min}$ observed for all of the fuels tested. $T_{ign,min}$ increases as the content of *iso*-octane increases, which is in-line with the previous observations on O_2 conversion suggesting

fuel reactivity decreases with increased branching. The same effect of fuel branching on ignition temperature was observed by [29, 31–33] for non-catalytic conditions, reported in section 2.1.

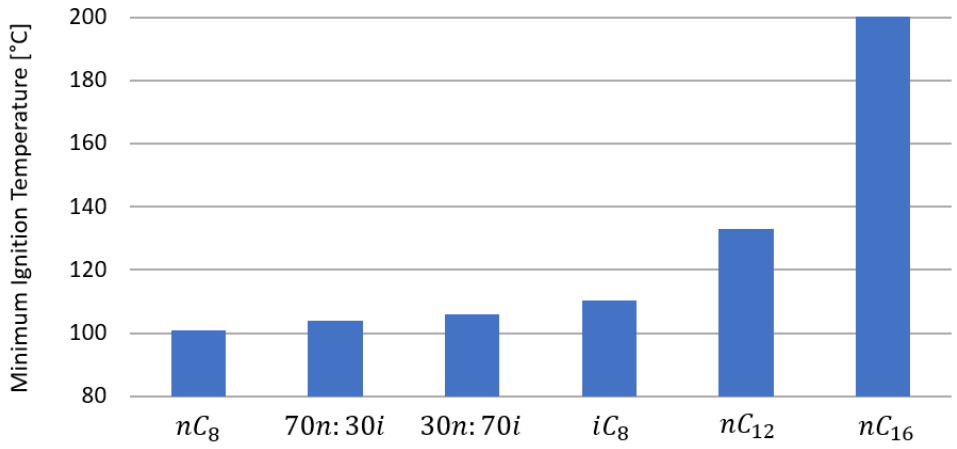

Figure 4.9: Average minimum igntion temperature for n-alkanes over Pt: ϕ=0.5, $\dot{V}_{air}$=9 sLpm, P=1 atm.

The back-face temperature of the catalyst for each fuel was plotted with respect to time during ignition in order to gain better understanding of how each fuel ignites. Fig. 4.10 shows this plot for select n-octane runs at various ignition temperatures. For the two low temperature runs, T_{ign}=111 and T_{ign}=121°C, a distinctive step occurs at $t \approx$25 s, which indicates a three-stage ignition process. Looking closely at the high temperature run (T_{ign}=140°C), a much smaller step occurs at $t \approx$20 s, suggesting that at even higher temperatures, the step would dissapear completely and n-octane would exhibit a purely single stage ignition.

Plots of back-face temperature as a function of time were also generated for *iso*-octane. Fig. 4.11 reveals a more distinct three-stage ignition process than n-octane.

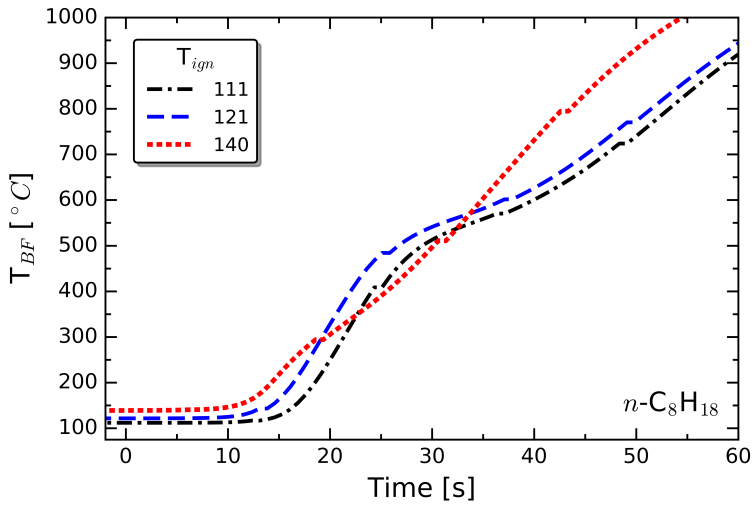

Figure 4.10: Backface temperature comparison for n-octane at different T_{ign}: ϕ=0.5, $\dot{V}_{air}$=9 sLpm, P=1 atm.

When compared to Fig. 4.10, the steps seen in Fig. 4.11, occurring from t =20-50 s, do not appear to change as T_{ign} increases. Plots of T_{BF} for the two octane mixtures are not shown, but they strongly resembled Fig. 4.11 for *iso*-octane, suggesting that the second stage is more sensitive to fuel branching. These observations are in line with those seen by Tekawade and Oehlschlaeger [29].

What follows is an explanation for the three-stage ignition process as well as the fundamental differences in behavior observed between n-octane and *iso*-octane. Using Fig. 4.12 for reference, (1) the fuel first begins to crack as it enters the reactor and continues cracking as it enters the catalytic foam. Once cracked, (2) the gas-phase intermediates adsorb onto the surface of the catalyst and ignite by consuming adsorbed O_2. There are however, a finite number of surface sites available on the catalyst, so some of the cracked intermediates (various hydrocarbons) must remain

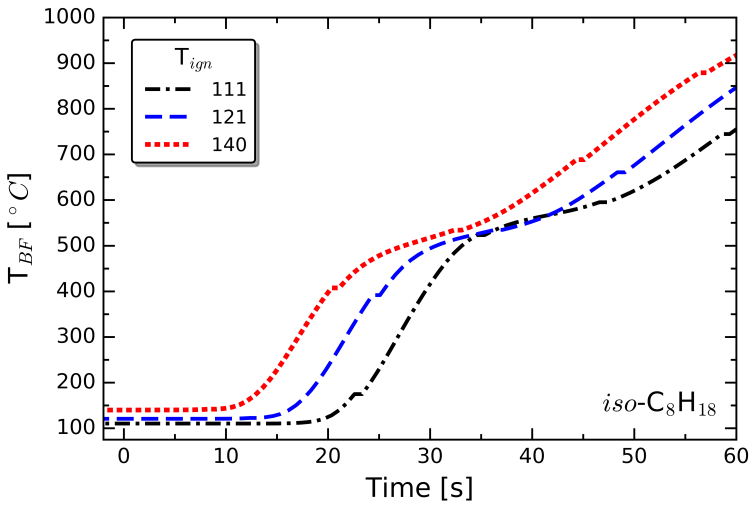

Figure 4.11: Backface temperature comparison for *iso*-octane at different T_{ign}: ϕ=0.5, $\dot{V}_{air}$=9 sLpm, P=1 atm.

in the gas-phase. Excess hydrocarbons greatly inhibit gas-phase CO oxidation [46] by combining with gas-phase O_2 to form compounds such as an alkyl-peroxyl radical [31], which is why CO is present during the ignition process in Figs. 4.4 - 4.7. Eventually the temperature becomes high enough that (3) CO can oxidize in the gas-phase, characterized by a sharp drop in CO and a corresponding increase in CO_2 production. As mentioned previously, the CO production is not constant across all four figures; it increases with increased branching. When cracked, *n*-alkanes can only ever form primary (single carbon) radicals (also called intermediates), while the branched nature of *iso*-octane can result in primary, secondary, and tertiary radicals. The secondary and tertiary radicals appear to dominate active sites on the catalyst and take longer to break down due to their more stable structure, which results in an overall slower ignition. With the slower active site turnover frequency

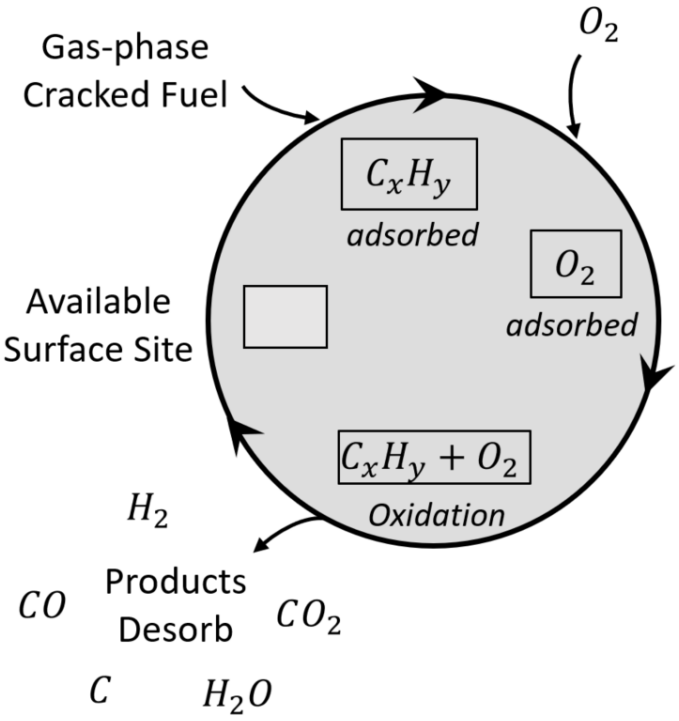

Figure 4.12: A diagram depeciting the typical hydrocarbon oxidation cycle seen on the surface of a catalyst.

of branched fuels, there are more hydrocarbons left in the gas-phase, resulting in less CO oxidation and increased amounts of CO observed in the product gas. In summary, the ignition process appears to be a three-stage process starting with gas-phase fuel cracking, heterogeneous oxidation of the cracked hydrocarbons, and gas-phase CO oxidation at sufficiently high temperatures ($T_{BF} > 700°C$). As mentioned previously, the equillibrium distributions seen in Fig. 4.8 for *iso*-octane agree well with the model, confirming that CO oxidation is the final step in achieving complete combustion.

The data collected for each fuel allowed for the calculation of E_a by way of the Arrhenius equation [46]

$$k = A \exp\left(- \frac{E_a}{R_u T} \right) \tag{4.1}$$

where k is the reaction rate, R_u is the universal gas constant, and T is the temperature. The E_a represents the amount of energy required to initiate a given reaction, such as oxidation. The term "global apparent activation energy" is used to in order to avoid confusion with true activation energy because global ignition properties were measured and used to calculate E_a by experimentally determining k as a function of T, where $T = T_{ign}$. Taking the natural logarithm of eqn. 4.1 gives

$$ln(k) = -\frac{E_a}{R_u T} + ln(A) \tag{4.2}$$

where E_a is easily found by plotting $ln(k)$ vs. $(R_u T)^{-1}$ and performing a linear regression, where $-E_a$ is equal to the slope of the best fit line. A function in the form of the Arrhenius equation can also be used to fit the data before the natural log is taken. Both methods were used to evaluate E_a as a way to check the calculations.

Assuming plug flow, first-order reaction with respect to O_2, constant catalyst surface temperature, decoupling of flow and temperature from steady state chemistry, and quasi-steady state surface coverages before lightoff, k can be determined using

$$k = \frac{-ln(1 - X_{O_2})}{t_{idt}} \tag{4.3}$$

where t_{idt} is the ignition delay time, and X_{O_2} is amount of oxygen conversion (mol%) that constitutes ignition [42]. Here, X_{O_2} =0.1, meaning that ignition is defined to

have occurred once O_2 conversion reaches 10% of its steady-state value. The t_{idt} was calculated by identifying and performing linear regression on the linear portion of the O_2 conversion curve and then using the obtained equation to solve for t_{idt} as seen in Fig. 4.13 (Note: not all data points are plotted for clarity). A Python code implementing the above equations was used to automate a large part of the data analysis and plotting.

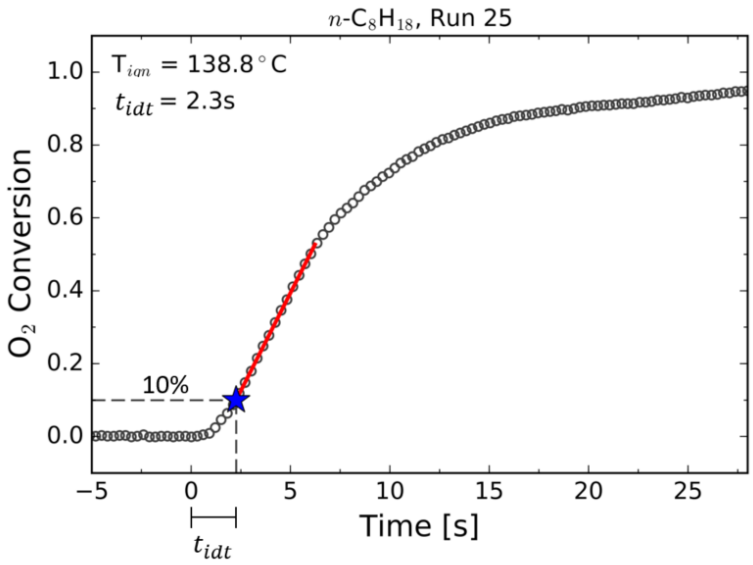

Figure 4.13: O_2 conversion illustrated to show determination of ignition delay time for n-octane, Run 25: ϕ=0.5, $\dot{V}_{air}$=9 sLpm, P=1 atm. Fuel is input at t=0 s.

Fig. 4.14 shows the Arrhenius plots for the four octane mixtures tested. The y-error bars and E_a values reported are for a 95% confidence interval (CI) from a least-squares analysis; x-errobars are not shown because all runs at a given temperature were typically within 1°C. The best-fit lines for all data plotted show linear correlation ($R^2 \geq 0.90$) between $ln(k)$ and T^{-1}, indicating reaction rate k is inde-

pendent of reactant concentrations and dependent only on temperature [46]. The E_a does not vary significantly for each octane mixture, particularly for mixtures containing *n*-octane, but there is a slight increase in E_a for pure *iso*-octane, indicating that fuel reactivity decreases with increased branching. More importantly, the presence of a catalyst significantly lowers the apparent activation energy of octane mixtures when compared to the average non-catalytic hydrocarbon activation energies reported in section 2.3. Quantitatively, a 61% decrease in E_a is seen when comparing the average octane mixture value to the non-catalytic hydrocarbon value given by Westbrook and Dryer [26].

4.1.1 Summary of Chain Branching Effects

The effect of chain branching on ignition characteristics and fuel reactivity were investigated using the CIET for four octane mixtures consisting of (*n*:*iso*) 100:0, 70:30, 30:70, and 0:100. A three-stage ignition consisting of gas-phase fuel cracking, heterogeneous hydrocarbon oxidation, and gas-phase CO oxidation was seen for all mixtures. The more distinctive steps in T_{BF} seen for mixtures containing *iso*-octane suggests the secondary and tertiary cracked intermediates dominate the active sites of the catalyst, resulting in a slower heterogeneous ignition process as observed in the O_2 conversion plots. These individual metrics indicate a decrease in reactivity with increased branching. When looking at the global reaction kinetics, however, the most important observation is that the presence of a catalyst significantly lowers the E_a of octane, making the energy requirement for ignition virtually the same for

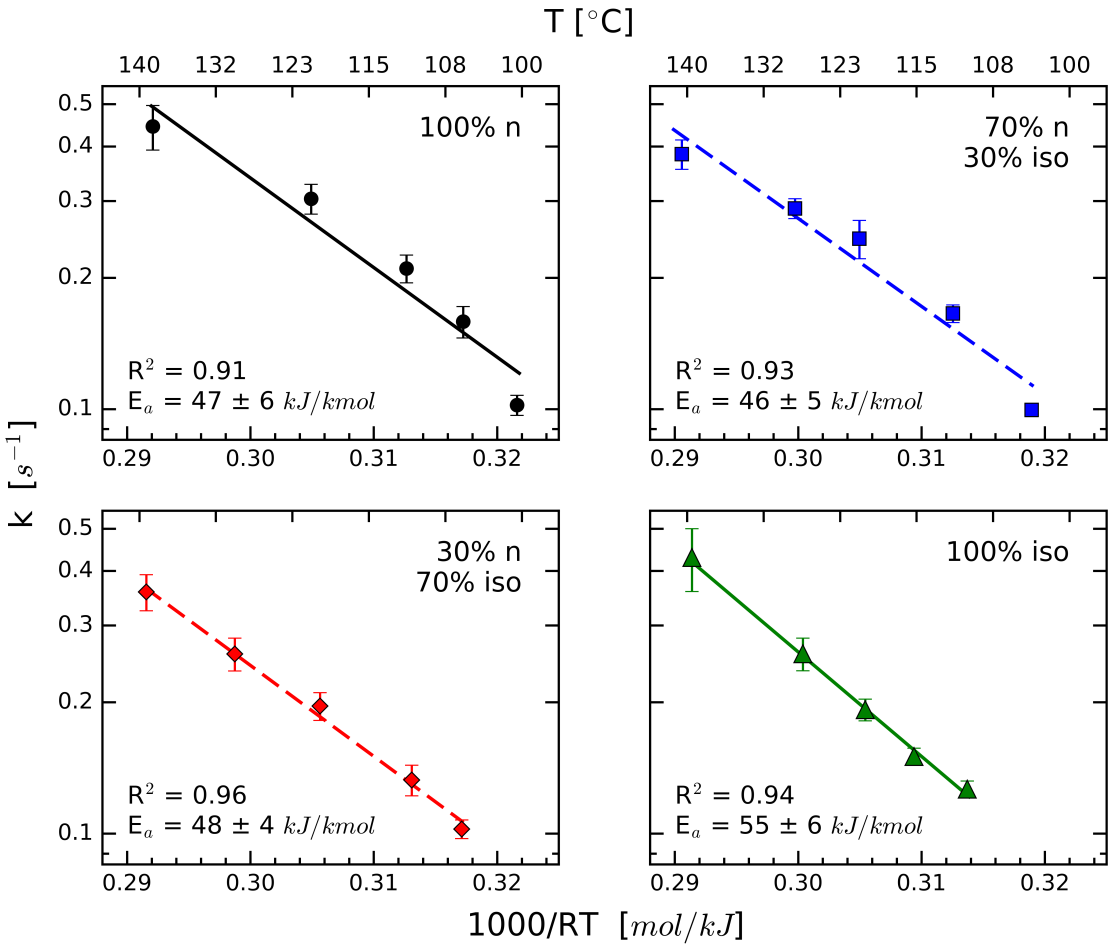

Figure 4.14: Arrhenius plot for the four octane mixtures tested. Error bars and reported E_a are for a 95% CI.

both straight-chained and branched fuels within experimental error, as seen in Table 4.1.

4.2 Chain Length Effects

The following section proceeds in a similar manner to the previous, 4.1, and discusses the observations and analysis concerning the effect n-alkane chain length

Table 4.1: Apparent global ignition parameters for the 6 fuels tested

Fuel	A_{mean} [s^{-1}]	$E_a \pm$ 95% CI [kJ/mol]
n-C_8H_{18}	6.5×10^4	47 ± 6
(70*n*:30*iso*) C_8H_{18}	4.3×10^4	46 ± 5
(30*n*:70*iso*) C_8H_{18}	2.6×10^5	48 ± 4
iso-C_8H_{18}	6.6×10^6	55 ± 6
n-$C_{12}H_{26}$	9.5×10^4	53 ± 2
n-$C_{16}H_{34}$	4.0×10^4	57 ± 4

on catalytic ignition. The fuels *n*-dodecane ($C_{12}H_{26}$) and *n*-hexadecane ($C_{16}H_{34}$), henceforth referred to as dodecane and hexadecane because neither of their isomers were tested, were chosen to compare to *n*-octane, a fuel whose results were discussed in the previous section. Dodecane and hexadecane have significantly higher boiling points, 216°C and 287°C, respectively, than *n*-octane and *iso*-octane, 125°C and 99°C, respectively, so all running conditions were kept at ϕ=0.5, $\dot{V}_{air}$=9 sLpm, P=1 atm, but the fuel preheat was increased for both dodecane and hexadecane to ensure adequate vaporization before making contact with the catalyst. As discussed in Ch. 2, the boiling point of a fuel has not been found to affect fuel reactivity, so the increased preheat is not expected to skew any results.

The O_2 conversion during the ignition of the three *n*-alkanes is compared in Fig. 4.15 and Fig. 4.16, where *iso*-octane is plotted as a solid line for reference. For the branched fuels comparison, $T_{ign,min}$ was nearly the same for every mixture, which resulted in a similar range of temperatures tested for each fuel. Looking at Fig. 4.9, it is clear that dodecane and hexadecane each have their respective temperature ranges for operation. The highest set of ignition temperatures tested, $T_{ign,high}$, and the middle temperature, defined as the average of $T_{ign,min}$ and $T_{ign,high}$,

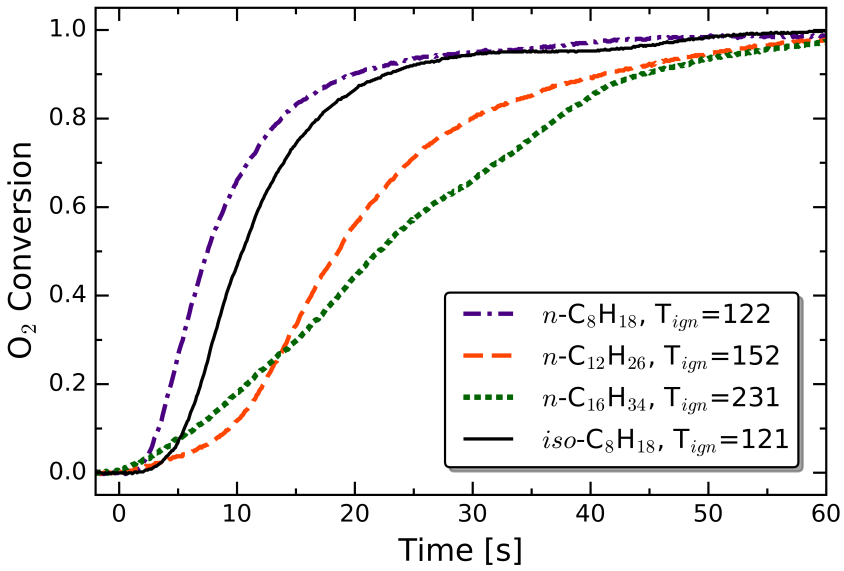

Figure 4.15: O_2 conversion comparison of n-alkanes at the middle ignition temperature ($\frac{1}{2}(T_{ign,high} - T_{ign,low})$) for ϕ=0.5, $\dot{V}_{air}$=9 sLpm, P=1 atm.

were chosen for each fuel to compare. The middle temperature runs, compared in Fig. 4.15, reveal a more constant ignition process for hexadecane, in that the rate of O_2 conversion does not vary much from X_{O_2}=0-0.8. Dodecane appears to behave more similarly to n-octane and *iso*-octane than it does to hexadecane. The same observations can be made looking at Fig. 4.16 for the high temperature runs. Dodecane exhibits a longer t_{idt} than hexadecane in both Fig. 4.15 and Fig. 4.16. The individual t_{idt} for each fuel, however, cannot be correlated to fuel reactivity due to the different temperature ranges required for testing the n-alkanes.

The CO_2 production seen in Fig. 4.17 and Fig. 4.18 for dodecane and hexadecane, respectively, correspond well with O_2 conversion plots shown previously. CO_2 production increases at a much more constant rate for hexadecane than for

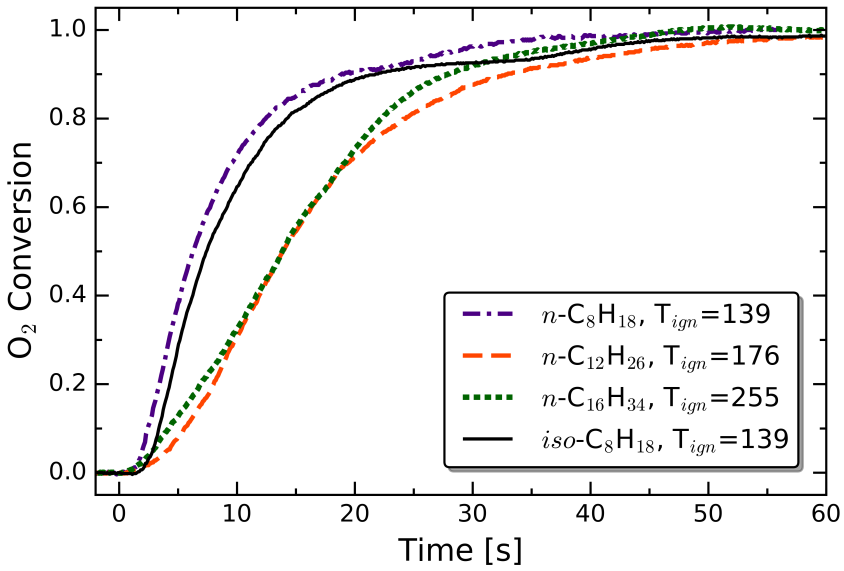

Figure 4.16: O_2 conversion comparison of n-alkanes at the highest ignition temperature for ϕ=0.5, $\dot{V}_{air}$=9 sLpm, P=1 atm.

dodecane. The H_2 and CO production for both fuels are approximately 0 during ignition, further strengthening the idea that H_2 and CO production observed during the ignition of the branched fuels is a result of the secondary and tertiary radicals dominating the catalyst active sites. With only primary radicals as a possibility, less CO is observed for the n-alkanes.

The equilibrium distribution of major combustion products was compared to a modeled equilibrium distribution using Cantera and reaction mechanism for n-dodecane for ϕ=0.5 [54]. Fig. 4.19 shows the experimental and modeled results after accounting for the absence of water. Both experiment and model are in good agreement, once again indicating that complete combustion occured despite the short contact times seen in the reactor.

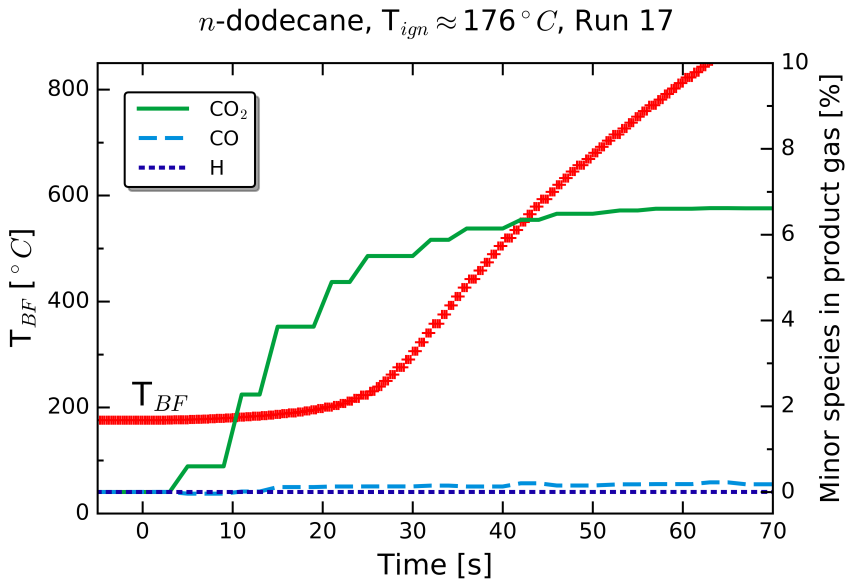

Figure 4.17: Minor species and T_{BF} of n-dodecane, Run 17: ϕ=0.5, $\dot{V}_{air}$=9 sLpm, P=1 atm.

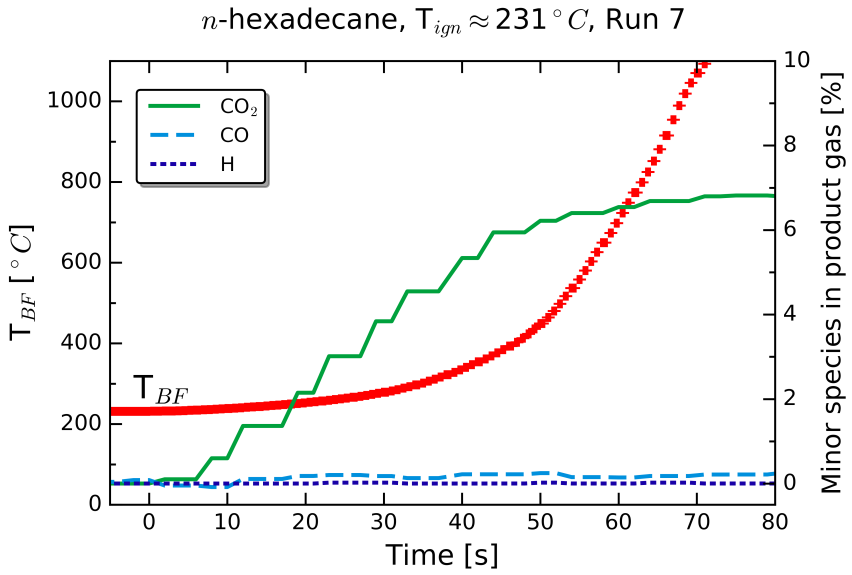

Figure 4.18: Minor species and T_{BF} of n-hexadecane, Run 7: for ϕ=0.5, $\dot{V}_{air}$=9 sLpm, P=1 atm.

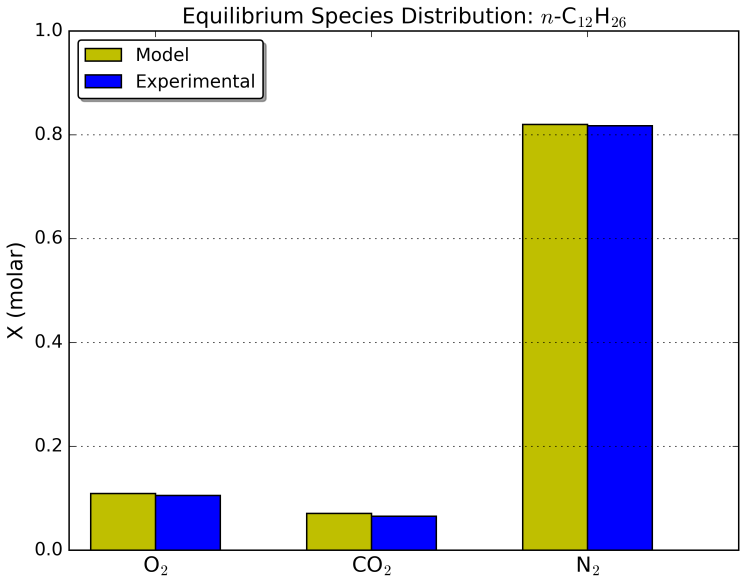

Figure 4.19: Model comparison of combustion product distribution n-dodecane. Experimental conditions for Run 3: T_{ign}=152°C, ϕ=0.5, $\dot{V}_{air}$=9 sLpm, P=1atm. Initial conditions for calculation: ϕ=0.5, T=27°C, P=1 atm

Looking at T_{BF} in Figs. 4.17 and 4.18, there is notable difference in the shape of each curve. These differences in behavior of T_{BF} for the two fuels become even more obvious when plotted for various T_{ign}, as seen in Fig. 4.20 and Fig. 4.21. For dodecane at lower ignition temperatures, T_{BF} increases at a nearly constant rate, but at T_{ign}=152°C, T_{BF} suddenly has two distinct linear regions. This profile was seen consistently in all five runs at T_{ign}=152. At the higher temperatures the linear regions become much less distinct but are still noticeable, especially for T_{ign}=164°C. The reason for the sudden change is unknown, but could be a consequence of the formation of site-blocking intermediates, which would result in an overall decrease in the rate CO_2 production, as observed.

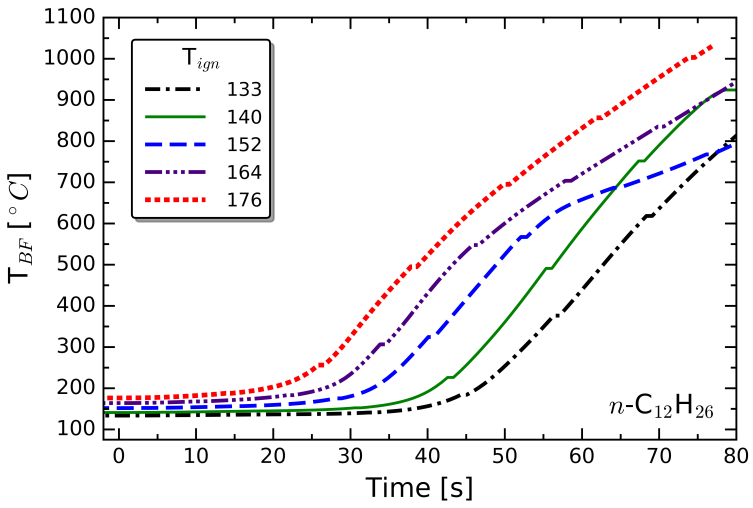

Figure 4.20: Backface temperature comparison for n-dodecane at different T_{ign}: ϕ=0.5, $\dot{V}_{air}$=9 sLpm, P=1 atm.

The T_{BF} for hexadecane, as seen in Fig. 4.21, is much different than any of the other fuels tested. The temperature slowly rises for anywhere from 40-70 s, and then increases at a rapid rate. The reason for this behavior is believed to be a result of short residence time. Just as with octane, hexadecane enters the reactor, begins to crack, and a portion of the cracked products adsorb onto the catalyst, continuing to break up and oxidize. The resulting heat from the exothermic heterogeneous reaction initiates the combustion of the gas-phase intermediates. However, due to the increased amount of time required to break the long intermediates up, combustion occurs more slowly, continuing further down the reactor.

As a way to partially validate the hypothesis above for hexadecane, T_{BF} and back shield temperature (T_{SB}) were plotted over the course of a run for T_{ign}=231°C. With combustion happening further down the reactor, it is expected that T_{SB} would

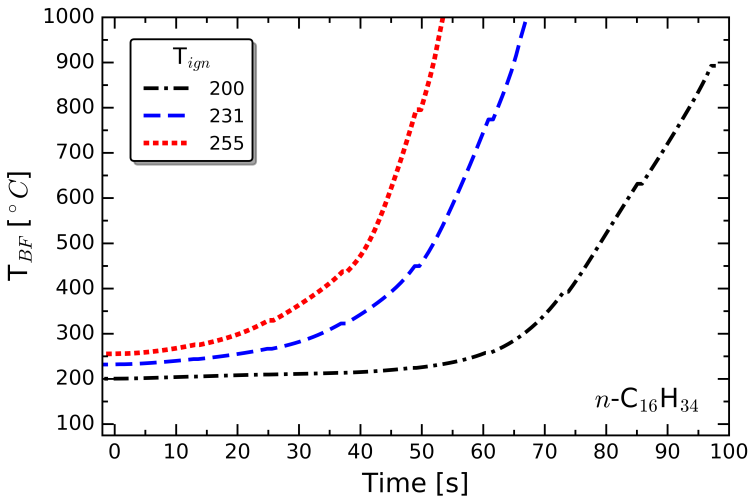

Figure 4.21: Backface temperature comparison for n-hexadecane at different T_{ign}: ϕ=0.5, $\dot{V}_{air}$=9 sLpm, P=1 atm.

remain higher than T_{BF} for a significant portion of ignition. The described trend can be seen for hexadecane in Fig. 4.22, and when compared to the Fig. 4.23, the same plot but for n-octane, it is easily seen that T_{SB} does indeed remain higher than T_{BF} for a significantly longer portion of ignition. The hexadecane T_{BF} overtakes T_{SB} at t=55s and a temperature of 600°C, while T_{BF} only takes about 17 s to surpass T_{SB} at a temperature of 200°C for n-octane. This prolonged combustion effect was also seen during experimentation. For the smaller fuels tested, T_{BF} would begin to fall almost immediately after fuel input was stopped. For hexadecane, however, T_{BF} would continue to rise for 5-10 s before beginning to fall. Further validation of the provided explanation requires additional experimentation. The same temperature comparison was also done for dodecane in the interest of completeness and can be found in Fig. 4.24. The temperature behavior during ignition for dodecane falls

in between that for n-octane and hexadecane, where T_{BF} overtakes T_{SB} at about t=42s and T=450°C.

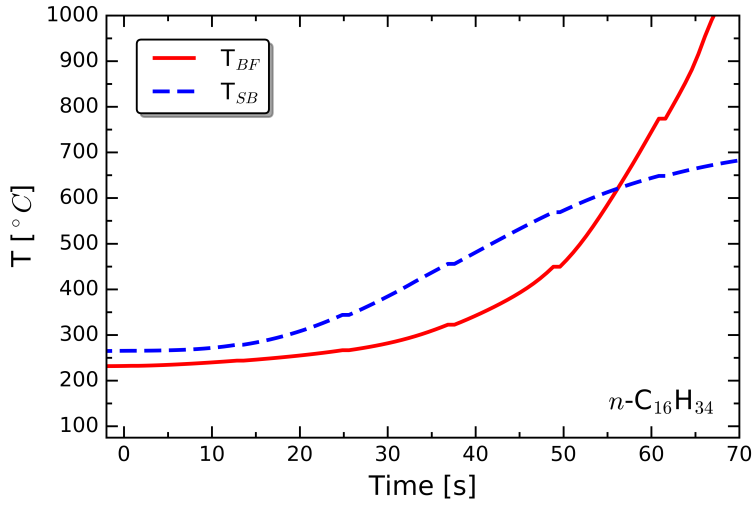

Figure 4.22: T_{BF} and T_{SB} for n-hexadecane, Run 7: ϕ=0.5, $\dot{V}_{air}$=9 sLpm, P=1 atm.

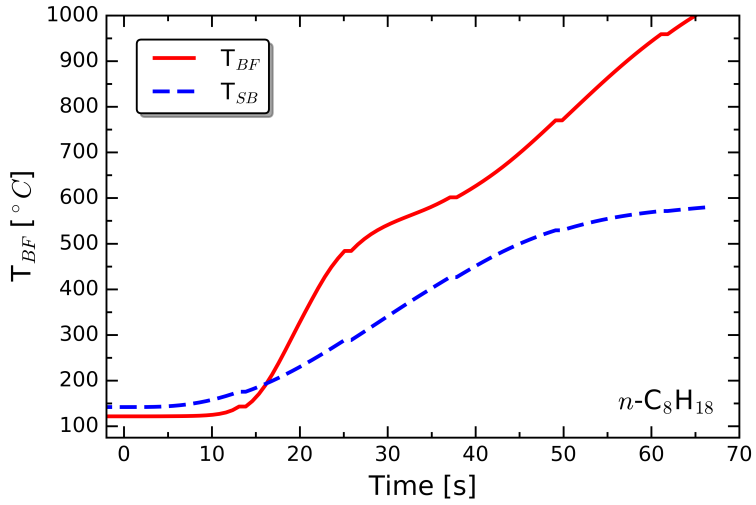

Figure 4.23: T_{BF} and T_{SB} for n-octane, Run 17: ϕ=0.5, $\dot{V}_{air}$=9 sLpm, P=1 atm.

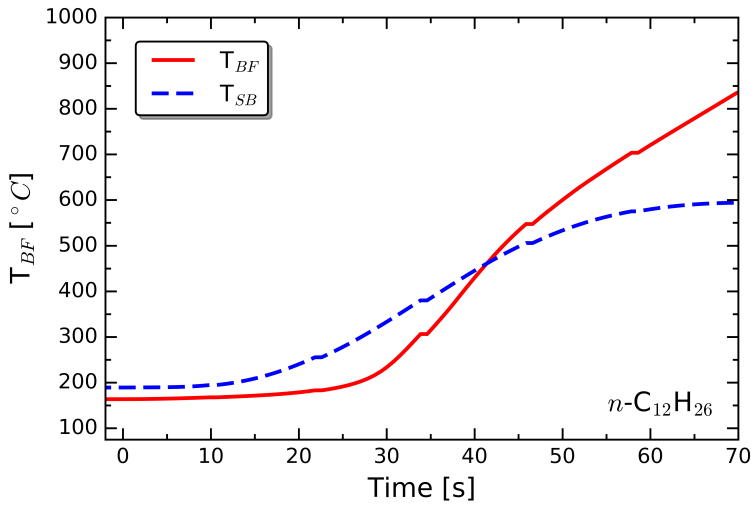

Figure 4.24: T_{BF} and T_{SB} for n-dodecane, Run 12: ϕ=0.5, $\dot{V}_{air}$=9 sLpm, P=1 atm.

The E_a for each fuel was determined using an Arrhenius plot as described previously in section 4.1. Due to the different operating temperature ranges, dodecane and hexadecane were plotted separately on Fig. 4.25 and Fig. 4.26, respectively. Looking at the error bars, again determined for a 95% CI, much less variation is seen between measurements across the entire temperature range as compared to the Arrhenius plots for the octane mixtures in Fig. 4.14. The calculated E_a values for each fuel, along with the global Arrhenius reaction parameters, can be found in Table 4.1. The E_a values for both dodecane and hexadecane are approximately the same as what was calculated for *iso*-octane. There is a slight decrease in E_a when compared to the fuels containing n-octane, which indicates that the ignition behavior of the longer n-alkanes and of pure *iso*-octane is more dependent on temperature than the fuels containing various amounts of shorter n-alkanes. Using the CIET to

test alkane mixtures of 30% n-octane and 70% n-dodecane as well as 30% n-octane and 70% n-hexadecane would provide more insight into how dominant the effect of shorter n-alkanes is on the observed E_a.

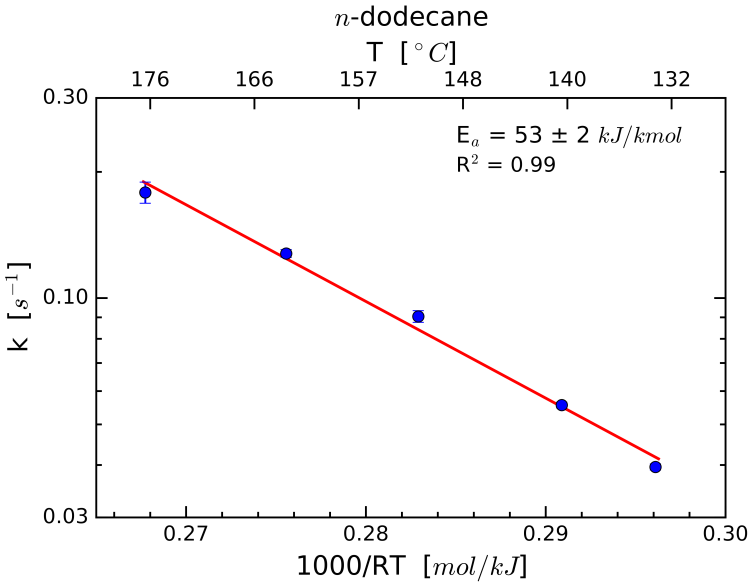

Figure 4.25: Arrhenius plot for n-dodecane. Error bars and reported E_a are for a 95% CI.

4.2.1 Summary of Chain Length Effects

The fuels n-octane, n-dodecane, and n-hexadecane were tested over a range of low ignition temperatures using the CIET to study the effect of chain length on ignition characteristics and fuel reactivity under low temperature, catalytic oxidation condtions. The smaller concentrations of H_2 and CO observed for the n-alkanes tested indicate high active site turnover frequency on the surface of the catalyst. Chain length greatly effects the back-face temperature of the catalyst during igni-

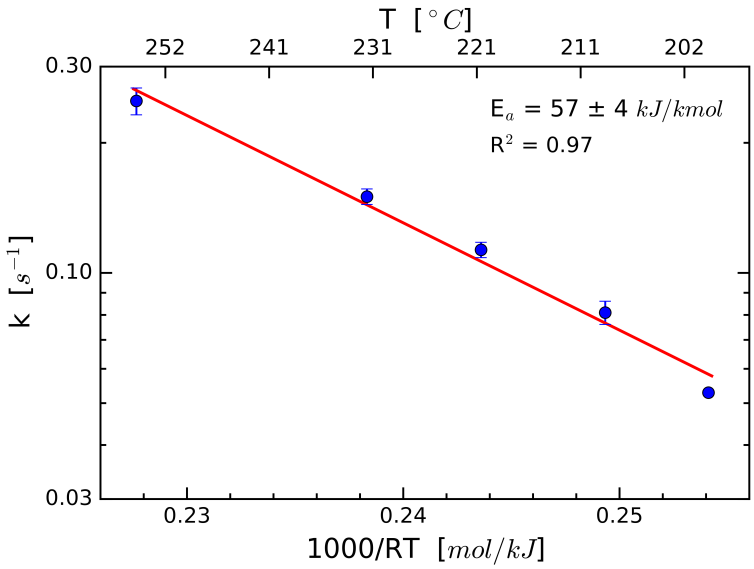

Figure 4.26: Arrhenius plot for n-hexadecane. Error bars and reported E_a are for a 95% CI.

tion. This is attributed to the combination of short residence times and the extra time required to break down longer fuel molecules. The E_a values calculated for dodecane (53 kJ/mol) and hexadecane (57 kJ/mol) are greater than that calculated for n-octane (47 kJ/mol), indicating an apparent increase in temperature sensitivity with increasing chain length. When compared to the non-catalytic hydrocarbon activation energies seen earlier, it is once again observed that the presence of a catalyst significantly lowers E_a.

Chapter 5: Conclusions

A CIET was developed as a way of testing the catalytic ignition behavior of liquid fuels at low temperatures and atmospheric pressure, a regime that has not been well studied or reported on in the past. The results of this experiment help fill an existing knowledge gap and can be used to help guide the design of catalytic micro-combustors as well as further the development of chemical models of catalytic hydrocarbon ignition.

The effects of chain branching on ignition were investigated by testing various mixtures of *n*-octane and *iso*-octane in the CIET. Fuel reactivity was shown to decrease with increased branching as indicated by the additional time required for O_2 conversion to take place at a given temperature for mixtures containing more *iso*-octane. $T_{ign,min}$ was also shown to increase slightly with increased branching.

Three fuels, *n*-octane, *n*-dodecane, and *n*-hexadecane were tested in the CIET to investigate the effect of chain length on ignition. The ignition behavior of hexadecane was the most unique out of all the fuels tested. This is likely due to the short residence times seen during experimentation coupled with the extra time required to break down the long fuel molecules. Comparing $T_{ign,min}$ does not appear to be a valid measure of fuel reactivity when comparing fuels of different chain lengths but

more a measure of the energy required to vaporize them. When comparing isomers of the same fuel, however, this issue is largely avoided.

Comparing the branched and straight chained results, branched isomers tend to behave more similarly to their straight chained counterparts in terms of O_2 conversion and temperature profiles during ignition. Less H_2 and CO production was observed during ignition for all n-alkanes tested, providing evidence of site blocking by secondary and tertiary radicals during ignition of the branched fuels, leading to a more distinct three stage ignition: gas-phase fuel cracking, heterogeneous hydrocarbon oxidation, and gas-phase CO oxidation. Considering the global ignition characteristics of single component fuels, increasing branching and chain length both appear to have the same effect and increase the apparent E_a. The presence of *n*-octane appears to negate the effect of branching and lowers the observed activation energies. Based on the data presented, it is also hypothesized that the presence of *n*-octane would lower the global activation energies of dodecane and hexadecane, negating the observed effect of chain length on E_a.

The range of activation energies calculated for the liquid alkanes tested in the CIET, 41-61 kJ/mol [1], were significantly lower than the reported range for non-catalytic hydrocarbon activation energies (109-167 kJ/mol) [47, 50], proving that proper implementation of a catalyst could greatly improve the start-up characteristics of micro-combustors.

[1] Lower and upper bounds of experimentally calculated activation energies for all fuels for a 95% CI

5.1 Recommendations for Future Work

There are many opportunities for future work in the area of low temperature, atmospheric, catalytic combustion. More fuels, gas and liquid, need to be tested at various equivalence ratios and contact times in order to better understand the effect fuel structure has on ignition. More specifically, *neo*-octane, which is more branched than *iso*-octane, could be incorporated into the octane mixtures presented here. Testing binary mixtures of *n*:*iso*, *n*:*neo*, and *iso*:*neo*, as well as mixtures of all three (*n*:*iso*:*neo*), would provide a more complete map of the effect of branching on ignition. Testing smaller alkanes such as methane and ethane would allow for more direct comparisons to past research as well as providing validation for existing chemical models.

In addition to testing pure component fuels, real fuels should be tested because that is what will ultimately be used in the field. Gasoline and synthetic jet fuels are good candidates because they do not contain sulfur and would therefore be less likely to deactivate the catalyst during testing. The results from the real fuels could be used to develop surrogate fuel mixtures, which are useful for modeling, device testing, and catalyst screening (testing different catalysts for use in a particular application). In regards to catalyst screening, the CIET could also be used for long-term tests to study catalyst deactivation under different conditions.

Appendix A: Supplemental Figures

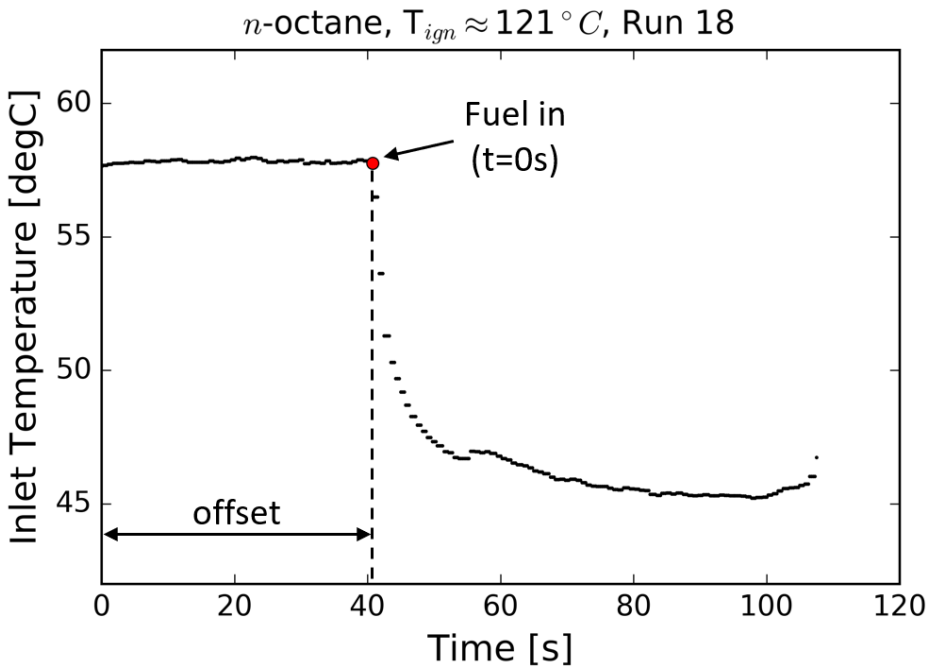

Figure A.1: Example inlet temperature plot illustrating how the "fuel in" time was detected. Experimental conditions for n-octane, Run 18: T_{ign}=121°C, ϕ=0.5, $\dot{V}_{air}$=9 sLpm, P=1atm.

Appendix B: Catalyst Preparation

1. Weigh and record the mass of each foam.
    - If making multiple catalysts, write on the bottom of a petri dish to keep track of each foam.
2. Mix alumina (2100) and distilled water in beaker. For an 80 ppi, 1"D x 1"L foam:
    - Use 5 mL of water (≈20 drops per mL).
    - Alumina powder should be ≈5% of the foam's mass.
3. Use a dropper to evenly distribute the alumina-water mixture onto the foam.
    - Flip the foam over after $\frac{1}{2}$ the mixture is used to avoid gumming up the surface.
4. Place foams in the furnace and bake at 700°C for 8 hr.
5. Weigh and record the mass of each foam
6. Use a dropper to distribute catalyst solution onto the foam
    - Solution: Pt Nitrate, Rh Nitrate, etc.
    - Place 15-20 evenly spaced drops on each face, let settle, and then place the foam on its side and apply a few drops in the middle.
7. Place foams in the furnace and bake at 700°C for 8 hr.
8. Weigh and record the final mass of each foam
    - Calculate the loading (%wt.) of the catalyst:

$$\%\ Loading = \frac{m_{final} - m_{step\,5}}{m_{step\,5}} \tag{B.1}$$

where m refers to the mass of the foam.

Appendix C: Ignition Temperature and Delay Time for Each Run

Table C.1: Data for n-C_8H_{18} and (70n:30iso) C_8H_{18}

Fuel: n-C_8H_{18}			Fuel: (70n:30iso) C_8H_{18}		
Run	T_{ign} [°C]	t_{idt} [s]	Run	T_{ign} [°C]	t_{idt} [s]
1	111	4.3	1	121	4.0
2	112	4.8	2	121	4.0
3	112	4.6	3	121	3.7
4	112	4.0	4	122	3.0
5	111	3.9	5	121	3.9
6	106	6.1	6	112	5.8
7	106	5.2	7	112	5.1
8	106	5.8	8	112	5.3
9	106	5.0	9	112	5.2
10	106	6.5	10	112	5.8
11	101	7.9	11	104	9.4
12	101	9.2	12	104	8.9
13	101	8.7	13	104	9.6
14	101	9.3	14	104	8.6
15	101	9.2	15	104	8.8
16	121	3.5	16	140	2.2
17	122	3.0	17	141	2.3
18	121	2.9	18	140	2.7
19	121	2.9	19	141	2.5
20	121	2.6	20	142	2.1
21	138	1.6	21	128	2.9
22	139	2.1	22	128	3.4
23	138	2.1	23	128	3.2
24	139	2.2	24	128	2.9
25	139	2.3	25	128	3.2

Table C.2: Data for (30n:70iso) C_8H_{18} and iso-C_8H_{18}

Fuel: (30n:70iso) C_8H_{18}			Fuel: iso-C_8H_{18}		
Run	T_{ign} [°C]	t_{idt} [s]	Run	T_{ign} [°C]	t_{idt} [s]
1	120	4.0	1	140	1.7
2	121	5.1	2	139	2.9
3	120	4.9	3	140	2.4
4	120	4.6	4	139	1.9
5	120	4.4	5	140	2.0
6	111	8.2	6	121	4.8
7	111	6.2	7	121	5.3
8	111	6.4	8	121	4.6
9	111	6.8	9	121	4.4
10	111	6.6	10	121	4.4
11	106	8.8	11	116	6.4
12	106	8.2	12	116	5.8
13	106	9.2	13	115	6.3
14	106	9.5	14	116	6.0
15	106	8.4	15	116	5.6
16	129	3.9	16	110	7.3
17	129	3.6	17	110	6.8
18	130	3.7	18	110	7.7
19	130	3.2	19	110	7.2
20	130	3.0	20	110	6.7
21	139	2.7	21	127	3.3
22	140	2.4	22	127	3.4
23	139	2.1	23	127	3.1
24	140	2.8	24	127	3.8
25	139	2.7	25	127	4.0

Table C.3: Data for n-$C_{12}H_{26}$ and n-$C_{16}H_{34}$

Fuel: n-$C_{12}H_{26}$			Fuel: n-$C_{16}H_{34}$		
Run	T_{ign} [°C]	t_{idt} [s]	Run	T_{ign} [°C]	t_{idt} [s]
1	151	9.8	1	221	7.9
2	151	10.4	2	220	8.3
3	152	9.5	3	221	7.8
4	153	9.7	4	220	8.4
5	152	10.4	5	221	7.4
6	141	16.1	6	232	5.7
7	140	15.7	7	232	5.6
8	140	16.6	8	231	6.0
9	140	16.2	9	231	6.4
10	140	16.3	10	231	6.2
11	163	6.9	11	255	3.9
12	163	7.3	12	255	3.7
13	164	6.9	13	255	4.0
14	164	6.9	14	255	3.4
15	163	7.2	15	255	3.2
16	176	4.9	16	209	10.7
17	176	5.2	17	209	9.9
18	176	5.3	18	209	11.8
19	176	4.5	19	209	11.6
20	176	5.4	20	209	11.8
21	133	22.8	21	200	17.0
22	133	22.1	22	200	17.4
23	133	22.8	23	200	16.8
24	133	22.8	24	200	16.9
25	133	23.4	25	200	17.0

Appendix D: Failed Experimental Operating Conditions

Table D.1: Select failed experimental conditions (P=1 atm)

Fuel	ϕ	$\dot{V}_{N2}$ [sLpm]	$\dot{V}_{O2}$ [sLpm]	T_{ign} [°C]	Reason Failed
n-octane	0.4	3.95	1.05	130-190	1
iso-octane	0.4	3.95	1.05	185-220	1
n-octane	0.8	7.11	1.89	105-145	2
n-octane	0.7	7.11	1.89	100	2
n-octane	0.5	7.11+2	1.89	112-170	3
n-dodecane	0.5	7.11+2	1.89	130-235	3

Reason Failed:

1. These results appeared to be diffusion limited (E_a ~0) and were characterized by ignition at the front face of the catalyst.

2. Steady state operation could not be achieved due to high temperatures which would have caused the catalyst to vaporize. This is a result of the increase in fuel flow rate.

3. Excess nitrogen was flowed in order to keep the temperature of the reactor lower. This resulted in incomplete combustion and is attributed to the lower temperatures and shortened residence times.

Bibliography

[1] M.E. LePera. The reality of the single-fuel concept. Army Logistician: `http://www.alu.army.mil/alog/issues/marapr05/reality.html`, 2005. Accessed: 2017-03-26.

[2] Allison Barrow. Fuel reformation. `http://science.dodlive.mil/2014/02/25/fuel-reformation/`, February 2014. Accessed: 2017-04-23.

[3] Joel Schmitigal and Jill Tebbe. Jp-8 and other military fuels. Technical report, U.S. Army TARDEC, 2011.

[4] Grant Dubé. Why and how jp-8 is being used on the battlefield today. Technical report, University of Maryland, 2017.

[5] Ivan C. Lee and Deryn Chu. Literature review of fuel processing. Technical report, U.S. Army Research Laboratory, March 2003. Report is distributed by the U.S. Army Research Laboratory.

[6] Thomas Reddy. *Linden's Handbook of Batteries, 4th Edition*. McGraw-Hill Education, 2010.

[7] James Huth and Josh Collins. 13th international stirling engine conference. In *Diesel fuel-to-electric energy conversion using compact, portable, stirling engine-based systems*. Stirling Engine Conference, 2007.

[8] CM Miesse, RI Masel, CD Jensen, MA Shannon, and M Short. Submillimeter-scale combustion. *AICHE JOURNAL*, 50(12):3206–3214, DEC 2004.

[9] Edward Shaffer and Tsvetanka Zheleva. Energy and power materials and devices science and technology. Expected publication date: May 2018.

[10] I.C. Lee, A.S. Gamon, and W.R. Allmon. Evaluation of a small prototype combustor. Technical report, Army Research Laboratory, 2011. ARL-TR-5738.

[11] G.J. Snyder. Thermoelectrics: The science of thermoelectric materials. Northwestern Materials Science and Engineering: `http://thermoelectrics.matsci.northwestern.edu/thermoelectrics/`. Date Accessed: 2017-04-21.

[12] Michael Mosburger, Jerry Fuschetto, Dennis N. Assanis, Zoran Filipi, and Heather McKee. Impact of high sulfur military JP-8 fuel on heavy duty diesel engine EGR cooler condensate. *SAE International Journal of Commercial Vehicles*, 1(1):100–107, apr 2008.

[13] Us: Fuels: Diesel and gasoline. https://www.transportpolicy.net/standard/us-fuels-diesel-and-gasoline/. Date Accessed: 2017-05-01.

[14] F.L. Dryer. Generation of comprehensive surrogate kinetic models and validation databases for simulating large molecular weight hydrocarbon fuels. Technical report, Princeton University, 2007.

[15] Bruno Kerschgens, Liming Cai, Heinz Pitsch, Benedikt Heuser, and Stefan Pischinger. Di-n-buthylether, n-octanol, and n-octane as fuel candidates for diesel engine combustion. *Combustion and Flame*, 163:66–78, 2016.

[16] Anand Krishnasamy, Rolf D Reitz, Werner Willems, and Eric Kurtz. Surrogate diesel fuel models for low temperature combustion. Technical report, SAE Technical Paper, 2013.

[17] Patrick Le Clercq, Massimiliano Di Domenico, Michael Rachner, Elizaveta Ivanova, and Manfred Aigner. Impact of fischer-tropsch fuels on aero-engine combustion performance. In *48th AIAA Aerospace Sciences Meeting Including the New Horizons Forum and Aerospace Exposition*, page 613, 2010.

[18] Patrick Le Clercq, Nicolas Doué, Michael Rachner, and Manfred Aigner. Validation of a multicomponent-fuel model for spray computations. In *47th AIAA Aerospace Sciences Meeting including The New Horizons Forum and Aerospace Exposition*, page 1188, 2009.

[19] Youngchul Ra and Rolf D. Reitz. A vaporization model for discrete multi-component fuel sprays. *International Journal of Multiphase Flow*, 35(2):101 – 117, 2009.

[20] Shiyou Yang, Youngchul Ra, Rolf D Reitz, Brad VanDerWege, and Jianwen Yi. Integration of a discrete multi-component fuel evaporation model with a g-equation flame propagation combustion model and its validation. *International Journal of Engine Research*, 13(4):370–384, 2012.

[21] Petroleum hydrocarbon ranges. ALS Environmental: `http://www.caslab.com/Petroleum-Hydrocarbon-Ranges/`. Accessed: 2017-04-23.

[22] K. Anand, Y. Ra, R. D. Reitz, and B. Bunting. Surrogate Model Development for Fuels for Advanced Combustion Engines. *ENERGY & FUELS*, 25(4):1474–1484, APR 2011.

[23] Frederick L. Dryer. Chemical kinetic and combustion characteristics of transportation fuels. *Proceedings of the Combustion Institute*, 35(1):117 – 144, 2015.

[24] Hsi-Ping S. Shen, Justin Steinberg, Jeremy Vanderover, and Matthew A. Oehlschlaeger. A shock tube study of the ignition of n-heptane, n-decane, n-dodecane, and n-tetradecane at elevated pressures. *Energy & Fuels*, 23(5):2482–2489, may 2009.

[25] HJ Curran, P Gaffuri, WJ Pitz, and CK Westbrook. A comprehensive modeling study of n-heptane oxidation. *COMBUSTION AND FLAME*, 114(1-2):149–177, JUL 1998.

[26] Charles K. Westbrook, William J. Pitz, Olivier Herbinet, Henry J. Curran, and Emma J. Silke. A comprehensive detailed chemical kinetic reaction mechanism for combustion of n-alkane hydrocarbons from n-octane to n-hexadecane. *COMBUSTION AND FLAME*, 156(1):181–199, JAN 2009.

[27] Eliseo Ranzi, Alessio Frassoldati, Silvia Granata, and Tiziano Faravelli. Wide-range kinetic modeling study of the pyrolysis, partial oxidation, and combustion of heavy n-alkanes. *Industrial & engineering chemistry research*, 44(14):5170–5183, 2005.

[28] Joffrey Biet, Mohammed Hichem Hakka, Valérie Warth, Pierre-Alexandre Glaude, and Frédérique Battin-Leclerc. Experimental and modeling study of the low-temperature oxidation of large alkanes. *Energy & Fuels*, 22(4):2258–2269, 2008.

[29] Aniket Tekawade and Matthew A. Oehlschlaeger. An experimental study of the spray ignition of alkanes. *Fuel*, 185:381 – 393, 2016.

[30] Jacob Mendelson. Ignition quality tester characterization with pure component and conventional navy fuels. Master's thesis, University of Maryland, Department of Mechanical Engineering, 2016.

[31] John Bugler, Brandon Marks, Olivier Mathieu, Rachel Archuleta, Alejandro Camou, Claire Grgoire, Karl A. Heufer, Eric L. Petersen, and Henry J. Curran. An ignition delay time and chemical kinetic modeling study of the pentane isomers. *Combustion and Flame*, 163:138 – 156, 2016.

[32] Wei Li, Guoqing Wang, Yuyang Li, Tianyu Li, Yan Zhang, Chuangchuang Cao, Jiabiao Zou, and Chung Law. Experimental and kinetic modeling investigation on pyrolysis and combustion of n-butane and i-butane at various pressures. *Combustion and Flame*, 191:126 – 141, 2018.

[33] SG Davis and CK Law. Determination of and fuel structure effects on laminar flame speeds of C-1 to C-8 hydrocarbons. *COMBUSTION SCIENCE AND TECHNOLOGY*, 140(1-6):427–449, 1998.

[34] Andrea Carrera, Matteo Pelucchi, Alessandro Stagni, Alessandra Beretta, and Gianpiero Groppi. Catalytic partial oxidation of n-octane and iso-octane: Experimental and modeling results. *International Journal of Hydrogen Energy*, 42(39):24675 – 24688, 2017.

[35] B.J. Dreyer, I.C. Lee, J.J. Krummenacher, and L.D. Schmidt. Autothermal steam reforming of higher hydrocarbons: n-decane, n-hexadecane, and jp-8. *Applied Catalysis A: General*, 307(2):184 – 194, 2006.

[36] Cline Hognon, Yves Simon, Paul-Marie Marquaire, Claire Courson, and Alain Kiennemann. Hydrogen production by catalytic partial oxidation of propane over ceo2. *Chemical Engineering Science*, 181:46 – 57, 2018.

[37] Jakob J. Krummenacher, Kevin N. West, and Lanny D. Schmidt. Catalytic partial oxidation of higher hydrocarbons at millisecond contact times: decane, hexadecane, and diesel fuel. *Journal of Catalysis*, 215(2):332 – 343, 2003.

[38] G.J. Panuccio, K.A. Williams, and L.D. Schmidt. Contributions of heterogeneous and homogeneous chemistry in the catalytic partial oxidation of octane isomers and mixtures on rhodium coated foams. *Chemical Engineering Science*, 61(13):4207 – 4219, 2006.

[39] Renate Schwiedernoch, Steffen Tischer, Chrys Correa, and Olaf Deutschmann. Experimental and numerical study on the transient behavior of partial oxidation of methane in a catalytic monolith. *Chemical Engineering Science*, 58(3):633 – 642, 2003. 17th International Symposium of Chemical Reaction Engineering (IS CRE 17).

[40] R. Subramanian, G.J. Panuccio, J.J. Krummenacher, I.C. Lee, and L.D. Schmidt. Catalytic partial oxidation of higher hydrocarbons: reactivities and selectivities of mixtures. *Chemical Engineering Science*, 59(22):5501 – 5507, 2004. ISCRE18.

[41] Kohei Urasaki, Shigeru Kado, Asako Kiryu, Ken ichi Imagawa, Keiichi Tomishige, Raimund Horn, Oliver Korup, and Yoshifumi Suehiro. Synthesis gas production by catalytic partial oxidation of natural gas using ceramic foam catalyst. *Catalysis Today*, 299:219 – 228, 2018. Special Issue of Catalysis Today for NGCS 11 Troms.

[42] Kenneth A. Williams and Lanny D. Schmidt. Catalytic autoignition of higher alkane partial oxidation on rh-coated foams. *Applied Catalysis A: General*, 299:30 – 45, 2006.

[43] Götz Veser, Murtaza Ziauddin, and Lanny D. Schmidt. Ignition in alkane oxidation on noble-metal catalysts. *Catalysis Today*, 47(1):219 – 228, 1999.

[44] Xing-Cai Guo and Robert J Madix. Dehydrogenation, hydrogenation, exchange and combustion reactions of aromatic hydrocarbons on pd (100). *Journal of the Chemical Society, Faraday Transactions*, 91(20):3685–3694, 1995.

[45] K. Bijjula and D.G. Vlachos. Catalytic ignition and autothermal combustion of jp-8 and its surrogates over a pt/-al2o3 catalyst. *Proceedings of the Combustion Institute*, 33(2):1801 – 1807, 2011.

[46] Kenneth Kuan yun Kuo. *Principles of Combustion*. Wiley-Interscience, 2005. p.233.

[47] P.L. Walker and C.C. Wright. Hydrocarbon burning velocities predicted by thermal versus diffusional mechanisms. *Journal of the American Chemical Society*, 74(15):3769–3771, 1952.

[48] Teresa A. Wierzbicki, Ivan C. Lee, and Ashwani K. Gupta. Combustion of propane with pt and rh catalysts in a meso-scale heat recirculating combustor. *Applied Energy*, 130:350 – 356, 2014.

[49] Charles K Westbrook and Frederick L Dryer. Simplified reaction mechanisms for the oxidation of hydrocarbon fuels in flames. *Combustion science and technology*, 27(1-2):31–43, 1981.

[50] John B. Fenn and Hartwell F. Calcote. Activation energies in high temperature combustion. *Symposium (International) on Combustion*, 4(1):231 – 239, 1953. Fourth Symposium (International) on Combustion.

[51] GC Bond. Kinetics of alkane reactions on metal catalysts: activation energies and the compensation effect. *CATALYSIS TODAY*, 49(1-3):41–48, FEB 24 1999. 1st Conference of the Indo-Pacific-Catalysis-Association, CAPE TOWN, SOUTH AFRICA, JAN 25-28, 1998.

[52] Jihad Ahmad Badra and Assaad R. Masri. Catalytic combustion of selected hydrocarbon fuels on platinum: Reactivity and heterohomogeneous interactions. *Combustion and Flame*, 159(2):817 – 831, 2012.

[53] Luong M.B., Luo Z., Lu T.F., Chung S.H., and Yoo C.S. Direct numerical simulations of the ignition of lean primary reference fuel/air mixtures under hcci condition. *Combust. Flame*, 2013.

[54] Zhaoyu Luo, Sibendu Som, S. Mani Sarathy, Max Plomer, William J. Pitz, Douglas E. Longman, and Tianfeng Lu. Development and validation of an n-dodecane skeletal mechanism for spray combustion applications. *Combustion Theory and Modelling*, 18(2):187–203, mar 2014.